HISTORY OF KINETIC POLAR WIND MODELS AND EARLY OBSERVATIONS

J.F. Lemaire, IASB & UCL, Belgium, lemaire@spaceradiations.be

W.K. Peterson, LASP, University of Colorado, bill.peterson@lasp.colorado.edu

T. Chang, MIT Kavli Institute for Astrophysics and Space Research,

Massachusetts, tsc@space.mit.edu

R.W. Schunk, CASS, Utah State University, schunk@cass.usu.edu

A.R. Barakat, CASS, Utah State University, barakat@cass.usu.edu

H.G. Demars, CASS, Utah State University, demars@cass.usu.edu

G.V. Khazanov, NSSTC/MSFC, Alabama, george.khazanov@nasa.gov

Abstract

Both the polar and solar winds were postulated to explain observations made before routine access to space was possible. Subsequently, significant limitations of the thermal plasma observations of the polar wind led to diverging approaches to modeling it. The hydrodynamic and kinetic approaches to modeling were able to explain the limited observational data. With no extensive and robust data set to determine the relative importance of dynamical effects in the ionosphere and convection in the magnetospheric electric field, there was no valid way to choose between the competing approaches. This has caused confusion in the space and plasma physics communities regarding the polar wind. Recent polar wind observations from the Japanese Akebono, NASA Polar, and the upcoming

Canadian e-POP missions call for an appropriate and timely review of our current understanding of the polar wind.

This paper presents a review of the modeling techniques from the earliest primitive approaches to the most current treatments that account for collision processes, non-Maxwellian distributions of multiple ion species, the role of photoelectrons in controlling plasma outflow and other topics. A brief overview of early polar wind measurements is given in Appendix B.

Keywords: Polar wind; Hydrodynamic models; Kinetic models; Plasma physics; Polar cap; Magnetosphere; Topside ionosphere; History of sciences

1. Introduction

The early years of space exploration were both exciting and confusing. Early ground-based research on radio wave propagation and cosmic rays had led to speculations about the space environment. Each instrument sent into space returned evidence of something unexpected. Investigations of the extension of the geomagnetic cavity and its comet-like tail in the anti-sunward direction, the apparent anomalous structure of the polar topside ionosphere, the nature of the plasmasphere, the origin of Carpenter's knee (plasmapause), and the relative concentration of helium isotopes in the atmosphere led early investigators in 1968 to postulate and start modeling what we now know as the polar wind to explain puzzling features and apparent inconsistencies in these early data sets. Confirming the existence and then systematically getting the data to characterize the polar wind proved to be a very challenging experimental task that is just now being completed using data obtained from the Akebono and Polar spacecraft.

The concept of a polar wind was introduced by Axford (1968) a decade after the existence of the solar wind had been predicted by Parker (1958) to model the supersonic expansion of plasma blowing out of the solar corona. The solar wind was also theoretically predicted to explain the motion of density irregularities

observed in cometary tails (e.g. Biermann, 1951, 1952). The solar wind (SW) is blowing into interplanetary space with supersonic bulk speed along open magnetic field lines. Since polar cap field lines are also 'open' and form the extended magnetospheric tail discovered by Ness (1965), it was tempting to predict the existence of a polar wind (PW) which is escaping out of the topside ionosphere above the polar caps and expanding with supersonic speed into the lobes of the magnetotail (Brinton et al., 1971; Nishida, 1966; Taylor et al., 1969). The polar wind depletes the high-latitude ionosphere of its content of light H^+ and He^+ ions and to some extent O^+ ions, thus forming the Light Ion Trough (LIT) as stressed by Taylor (1972).

The polar wind outflow was first modeled by Banks and Holzer (1968, 1969a,b), Marubashi (1970), and Banks et al. (1971) by solving the hydrodynamic continuity and momentum transport equations. The plasma was assumed to be isothermal, and the Euler approximation was used for the transport equations, even at high altitudes where the O^+ and H^+ thermal ions are almost collisionless. The distribution of density and bulk velocity of these ion species were obtained. Hydrodynamic friction in the momentum equation was thought to accelerate the field-aligned H^+ outflows once the inhibiting effect of H^+ - O^+ Coulomb collisions is reduced at higher altitudes. This model emphasized the subsonic-supersonic transition of this flow of ionospheric thermal ions. It is important to note that the state-of-the-art in thermal plasma measurements has only recently developed to the point that synoptic data sets from the Akebono and Polar satellites are available to rigorously constrain polar wind models. Refer to Appendix B for an extended discussion of early polar wind measurements.

The effects of energy and heat transfer processes in the hydrodynamic approach were included by Holzer et al. (1971) and others, in order to study the ion pressure and temperature anisotropies in the polar wind. The assumption of isothermal and isotropic temperatures was relaxed in these subsequent and more

sophisticated models which paved the way for many other steady state and time dependent transport PW models based on a variety of approximations and assumptions [reviewed by Schunk (1986, 1988) for the period before 1988, and by Ganguli (1996) for the following decade]. For more detailed accounts, these comprehensive reviews are recommended. After first recalling the main steps of polar wind history, the latest theoretical contributions in this field will be outlined.

Like the first hydrodynamic models of the solar wind, those of the polar wind quickly became very popular because of a historical controversy that occurred soon after their introduction by Banks and Holzer (1968). This historical debate opposed on one side (i) those promoting fluid descriptions – similar to those used in the 1950's to model the streamlines of highly conducting Mercury (Hg) flowing across magnetic fields in laboratory experiments, and on the other side (ii) those bringing up kinetic descriptions for collisionless plasmas flowing out of the ionosphere of the Earth or out of the solar corona. This debate has confused and provoked students for over four decades. It is still dividing the space plasma community. Not only did this confusion undermine progress in the understanding of the polar wind, but also left an aftermath that continues to puzzle scientists outside the space plasma community. Instead of acknowledging the remarkable complementarities of both approaches, the partisans on each side exclusively emphasize their differences and limitations. However, the resistance in both camps is gradually decreasing. The purpose of this paper is to present a balanced account of forty years of kinetic polar wind modeling efforts and to identify areas where the new synoptic data sets from Akebono and Polar can be used to increase understanding of the polar wind.

Before attempting to disentangle these lasting disagreements, let's review the roots of the PW history, which can be traced back into the 1950's, i.e. even before the discovery of the solar wind of which the polar wind appeared to be a possible hydrodynamic imitation. But is the PW acceleration really generated by the same

physical mechanism as the SW acceleration? This will be explored in the next sections.

2. Development of the polar wind concept

Aldrich and Neir (1948) reported the ratio of $^3He/^4He$ in various materials, as well as the Earth's atmosphere, as one of the first applications of the then evolving field of mass spectrometry. They confirmed the earlier report of Alvarez and Cornog (1939) that the ratio of $^3He/^4He$ was significantly different in samples taken from the air than those taken from wells. Nicolet (1957, 1961) examined the sources and losses for the two isotopes of helium found in the atmosphere: (i) radioactive decay of mantle material for ^4He, and (ii) cosmic rays for ^3He. Nicolet considered only the Jeans thermal escape mechanism for neutral helium atoms above the exobase as a loss process. He noted that the production rate of atmospheric ^4He by radioactive decay of uranium and thorium in the Earth's mantle and crust is greatly in excess of the thermal escape rate. The observed $^3He/^4He$ ratio was not compatible with a single He temperature and a Maxwellian particle velocity distribution function at the exobase.

Bates and McDowell (1957, 1959) and Bates and Patterson (1962) also addressed the need for an additional mechanism for He escape. They proposed dissociative recombination of HeO^+ as the source of non-thermal He. Since the photoionization rate of ^4He is equal to its production rate, Nicolet (1961) argued that terrestrial helium should mainly escape in its ionized state (see also Kockarts and Nicolet, 1962). Independently, Wilson (1962) suggested the loss of helium by direct production of He^+ by photoionization and its subsequent escape from the ionosphere.

MacDonald (1963) provided a comprehensive review of the helium problem. In particular, he systematically examined many proposed mechanisms put forward to resolve the problem. The result of MacDonald's analysis was inconclusive. A

subsequent review of this problem by Kockarts (1973) reached similar conclusions.

After the first observations from rockets and satellites were obtained, many new ideas circulated. Dungey (1961) proposed that the magnetosphere was coupled to the solar wind through magnetic reconnection. Axford and Hines (1961) introduced the concept of magnetospheric convection. Carpenter (1963) reported systematic observations of a density step (i.e. knee) in the plasma density as a function of radial distance. The composition of the topside ionosphere was addressed by many early investigators. Bauer (1966) noted that minor ions such as He^+ behave fundamentally different than the major ions. Other investigators, such as Dessler and Michel (1966), suggested that escape of significant fluxes of ions from the polar cap into the magnetotail was a basic property of the magnetosphere.

Nishida (1966) had the critical insight that eventually led to early polar wind models. In his 1966 paper, Nishida showed how magnetospheric convection and thermal plasma escape – in what has come to be called the polar wind – together are responsible for the reduction of light ion concentration from the topside ionosphere above the polar caps. This remarkable paper also presented a potential resolution of the helium problem, a better understanding of the topside ionosphere composition, beginnings of our understanding of the ionospheric contributions to the magnetosphere and for plasma sheet as well as the dynamics of the magnetosphere, and a possible mechanism for the formation of the plasmapause (Carpenter's knee).

The term "polar wind" first appeared in titles of two papers in the November 1968 issue of the *J. of Geophys. Res.*, by Axford (1968) and Banks and Holzer (1968). In later papers Banks and Holzer (1969a,b) attributed the term polar wind to Axford. The latter pointed out how the plasma escape postulated by Nishida (1966) could possibly resolve the helium problem. But subsequently, Kockarts

(1973) showed that although the PW helps to increase the escape of helium from the atmosphere, it is not sufficient, however, to evacuate all the helium atoms penetrating the bottom of the atmosphere due to radioactive decay of mantle material.

Banks and Holzer emphasized plasma transport and the structure of the topside ionosphere. Their numerical calculations were based on the hydrodynamic mass and momentum transport equations analogous to those used a decade earlier by Parker (1958) to model the plasma expansion and the structure of the solar corona. The hydrodynamic model of Banks and Holzer will be discussed in more detail because of its historical interest. Indeed, this early model has been the first of a series of more sophisticated models based on other more sophisticated approximations of the transport equations (Navier-Stokes approximation; Grads 5-, 8-, 13- or 20- moments approximations; …) that are discussed further by Ganguli (1996) as well as Tam et al. (2006) in this issue.

3. Early ideas and first hydrodynamic models of the polar wind

As already indicated, Banks and Holzer (1968) proposed the first hydrodynamic model for polar wind outward-flowing plasma. They justified the large upward acceleration of the H^+ ions into the supersonic flow regime as, "closely analogous to the expansion of the solar corona into interplanetary space as the solar wind. The use of friction and particle production and loss terms taken into account in the ion equations of momentum transport represents an extension of the conventional solar wind model to the more complicated ionospheric conditions". However, this mechanism they claimed to be "the basic physics of the polar wind plasma flow" was considered questionable by Dessler and Cloutier (1969), since it occurs in the exosphere where the effect of Coulomb collisions is negligibly small; the latter argued that the concept of "hydrodynamic flow only clouds the true physical picture…".

In the model of Banks and Holzer the electrons and ions have the same bulk velocity and form a single neutral fluid or plasma, just as if they were bound like in neutral atoms. The bulk velocities of the electrons and ions are meant to be their common average velocities. The distributions of the plasma density and bulk velocity are derived by integrating the Euler approximation of the single fluid transport equations under the assumption that the temperature distribution is independent of the altitude. Among the infinite set of steady state hydrodynamic solutions, Banks and Holzer (1968) selected the unique mathematical solution of the non-linear Euler transport equations that passes through a critical point of singularity. This critical solution is indeed the only steady state one that corresponds to a negligibly small plasma pressure at a large distance from the Earth. This solution is subsonic at low altitude and becomes a supersonic flow at large distances along the open magnetotail field lines. Fig. 1 illustrates the Mach number of all different families of solutions of the hydrodynamic transport equations applied by these authors to model the polar wind. The thick curve labeled A corresponds to the critical solution which is the only one that gives subsonic expansion velocities at low altitudes, and zero kinetic pressure at infinity. The temperature was assumed to be 3000 K and uniform (i.e. independent of altitude). The temperature of the neutral atoms used to evaluate the production and recombination rates of oxygen and hydrogen ions by resonant charge exchange reaction between O^+ and H was assumed to be 1000 K.

Soon after the publication of Banks and Holtzer's hydrodynamic polar wind model, Marubashi (1970) critically analyzed the hydrodynamic treatment for the motion of ions and electrons escaping from the polar ionosphere into the magnetospheric tail. It is unfortunate that Marubashi's contribution has not received the attention it deserves. Indeed, much of the controversy between the hydrodynamic and kinetic schools of thoughts could possibly have been avoided. The reader interested in understanding more precisely the "hydrodynamic

acceleration mechanism" of the polar wind, as well as the limitations of this approximation, should consult Marubashi's comprehensive article.

As discussed in Appendix B, only recently have reliable synoptic observations of the altitude dependence of the thermal plasma properties of the polar wind become available to test and constrain models such as the one proposed by Banks and Holzer.

4. A controversy: the validity of hydrodynamic approximations

Soon after the publication of the first hydrodynamic polar wind models, a passionate controversy began. This debate recalled another historical one that opposed, a decade earlier, the father of the first hydrodynamic model of the solar wind and the initiator of the challenging evaporative solar breeze model (Parker, 1958; Chamberlain, 1960).

Dessler and Cloutier (1969) pointed out that "the evaporative solution correctly describes the flow of neutral atomic hydrogen away from the Earth (the geocorona); the hydrodynamic solution does not". They considered that the same argument holds for ionized hydrogen flowing away from the Earth. They further argued that the hydrodynamic solution proposed by Banks and Holzer for the PW was inappropriate to model this flow above an exobase altitude.

The exobase level is defined as the altitude where the Coulomb collision mean-free-path of the hydrogen ions becomes equal to the density scale height of the oxygen ions that are still the major constituent at this altitude over the polar cap regions. This level is also often called the baropause, a usage introduced by pioneers like Spitzer (1949) and Jeans (1954) who studied the evaporation/escape of neutral atoms from the upper atmosphere of planets.

At the exobase the Knudsen number (i.e. the ratio of the mean-free-path of particles to the atmospheric density scale height) for the major ion species changes from values smaller than unity to values larger than 1. The exobase is located between 1500 and 3000 km altitude over the polar caps. Note that the

exobase for neutrals is 500-600 km, while the exobase for the ions is over 1000 km higher due to the larger Coulomb collision cross-section[♦].

The region above the exobase is the ion-exosphere. In the absence of binary collisions and other scattering mechanisms – e.g. wave-particle interactions which are ignored in exospheric models – the ions and electrons are free to spiral along the geomagnetic field lines. Due to the divergence of these field lines, charged particles experience the upward directed magnetic mirror force. Furthermore, upward moving ions are decelerated by the action of the gravitational force, but they are accelerated away from the exobase by the upward pointing polarization or ambipolar electric field whose origin is discussed in Appendix A, where we show that in a plasma in hydrostatic equilibrium in a gravitational field the polarization electric field corresponds to the Pannekoek-Rosseland electric field. The upward directed force (e **E**) on a singly charged O^+ ion is then equal to half the downward gravitational force (m **g**). Therefore, for the O^+ ions the sum of the electric and gravitational forces is directed downward and equal to half of the gravitational force on a neutral oxygen atom. However, for the H^+ and He^+ ions the total force is pointing away from the Earth, since the downward gravitational force on these ions is much smaller than the upward directed electric force on these ions which are lighter than O^+. This is precisely the force that, according to Dessler and Cloutier (1969), is responsible for the acceleration of the H^+ and He^+ ions out of the polar ionosphere. A thorough discussion and review of this

---

♦ The first exospheric density distribution for neutral atoms was developed by Öpik and Singer (1959, 1960, 1961). They showed that the barometric formula, used in all atmospheric models before 1960, does not correspond to the correct density distribution in the exosphere of the Earth (see Singer [1960] for a discussion on this question). See also Lemaire and Scherer (1974a), Fahr and Shizgal (1983), Shizgal and Arkos (1996) for successive updates on exospheric methods, model assumptions and results.

We note that available neutral density observations were made mostly in the 1970's from the Atmosphere Explorer mission and are available primarily through empirical model outputs as average parameters that do not reflect the dynamic variations in densities above 1000 km.

historical controversy can be found in Donahue (1971), and Lemaire and Scherer (1973).

Marubashi (1970) confirmed that an effective collision frequency about 10 times larger than the actual classical Coulomb collision frequency would be required for the Euler approximation to be valid throughout the outermost PW regions of the ionosphere. In his seminal paper he also presented the major advantages of an evaporative approach like that of Dessler and Cloutier. Unfortunately, in the arena of magnetohydrodynamics (MHD) little attention was paid to these relevant ideas.

5. First generation of kinetic polar wind models

Dessler and Cloutier (1969) did not just criticize the recent hydrodynamic model put forward by Banks and Holzer, but they offered an alternative model based on kinetic theory. Their kinetic model was an exospheric one, like the "solar breeze" model proposed by Chamberlain (1960) for the solar corona ten years earlier. For this reason they called their exospheric model "polar breeze". In exospheric models, unlike in any fluid approach, binary Coulomb collisions are completely ignored, at least beyond the critical altitude, which include the exobase or baropause altitude.

At the exobase, Dessler and Cloutier (1969) assumed that the velocity distribution function of the H^+ ions is mono-energetic with only upward moving velocities equal to the thermal speed, $(8kT/\pi m_H)^{1/2}$, where m_H is the mass of the hydrogen ions and T their temperature.

In the collision-dominated region, below the exobase where the Knudsen number is smaller than unity, the mean upward velocity of the light ions due to the acceleration by the electric field and gravity can be approximated by

$$\bar{\mathbf{v}}_{H^+} = \frac{1}{m_{H^+}}\left(\frac{m_{O^+}}{2} - m_{H^+}\right) g\,\tau_{H^+} \qquad (1)$$

where τ_{H^+} is the collision time for the H^+ of mass m_{H^+} embedded in a plasma where the O^+ ions are dominant. Thus, at the exobase the H^+ ions already have an average upward bulk speed of the order of $\bar{\mathbf{v}}_{H^+}$.

Above the exobase the H^+ ions are accelerated upward along the field lines as a result of the polarization electric field. When they encounter weaker magnetic fields at higher altitudes, they become more field-aligned. As a consequence of electric field acceleration and pitch angle change, the bulk velocity of the H^+ ions increases continuously to supersonic values in the distant ion-exosphere. Pitch angle scattering mechanisms feeding particles into the downward loss cone are assumed negligible. This assumption in exospheric models implies that the pitch angle distributions of charged particles are truncated or partly empty. The Liouville theorem can then be used to determine the velocity and pitch angle distribution of the H^+ ions everywhere else above the exobase, once it is determined at the exobase.

Using these simple assumptions Dessler and Cloutier (1969) showed that it is the upward directed polarization electric force that accelerates the light ions to supersonic wind bulk velocities in the topside polar ionosphere. This electric force is indeed explicitly present in the momentum equation for the electrons and for all ion species, but it does not appear in the one-fluid hydrodynamic polar wind model of Banks and Holzer (1968). Indeed, by combining the momentum equations for the electrons and for the ions the net electric force density vanishes since the plasma is assumed to be quasi-neutral. This was the mistaken reason why advocates of hydrodynamic or fluid descriptions of the polar wind and solar

wind argue that these flows are not accelerated by an electric field. [#] The counter argument is that the electric force accelerating the PW ions is definitely hidden in the single fluid formulation of the momentum equation within the total kinetic pressure gradient force term. In fact, this hydrodynamic pressure force includes the electron pressure which can be approximated by:

$$\nabla p_e \cong - n_e e E_{in} \qquad (2)$$

This equation is a simplified form of the electron momentum equation, wherein, due to their small mass, the inertial and gravitational forces acting on the electrons have been neglected compared to all other terms in the momentum equation. As a matter of consequence, the polarization electric force accelerating the PW flow is indeed present in the single fluid formulation, although it does not show up explicitly in standard one-fluid or MHD formulations of the plasma transport equations.[◊]

[#] In the one-fluid hydrodynamic approach, plasma is accelerated upward because the gradient of the total thermal pressure of the ions and electrons exceeds the gravitational term in the momentum transport equation.

[◊] According to Parker (2000, personal communication), *"the role of the electric field is to tie the electrons and ions together, so that their combined kinetic energies at the exosphere are available to boost the ions out of the gravitational field"*. In other words, he does not consider that thermal electrons are free to move in solar wind or polar wind independently from the ions, nor are they free to escape (runaway) out of gravitational plus electric potential well independently from the heavier and slower thermal ions. Following this erroneous interpretation the internal polarization electric field induced within plasmas should be identical to the Coulomb electric field tying bound electrons to the nucleus of neutral atoms. This fails be a correct statement as soon as the temperature of the gas exceeds its ionization temperature, i.e. when the outermost electrons are no more tied/bound to the nucleus of the atoms or ions.

The correct origin and build up of polarization electric fields inside a plasma due to plasma flow has lately been put forward by Vasyliunas (2001). He correctly shows the basic role played by the minute displacement currents in generating the so-called "internal convection electric field". This electric field is perpendicular to the magnetic field direction and to the direction of the plasma flow. Similarly, the gravitational and "centrifugal" forces as well as unequal diffusion fluxes or escape fluxes of electrons and ions (thermoelectric effect) generate internal polarization electric fields that may have a non-zero field-aligned component like for instance the Pannekoek-Rosseland electric field or that which accelerates the polar and solar winds ions to supersonic velocities.

Note that in the ideal MHD approximation both the field-aligned electric fields intensity and the displacement current are both assumed to be strictly nil. These are precisely the main flaws and basic drawbacks of ideal MHD theory, often applied to model the transport of plasma parallel and perpendicular to magnetic field lines.

It is therefore inappropriate to argue that the polar wind and solar wind ions are not accelerated by the internal (polarization or ambipolar) electric field induced within the plasma material either by gravity, thermoelectric effect, velocity shears, or any other physical effect producing a gradient in the electronic kinetic pressure, according to Eq. (2). Note that this is an internal electric field, and that any externally applied electric field ($\mathbf{E}_{ex}$) would not be able to accelerate the plasma neither parallel to magnetic field lines nor perpendicular to **B**. An externally applied electric field along **B** would produce a current, not a bulk motion of the electron-ion plasma. A simple physical explanation for the origin of the internal electric field generated inside a plasma element moving and accelerated across B-lines, can be found in Chandrasekhar's lectures in plasma physics; these were published in 1960 in a booklet titled *Plasma Physics*. This explanation is based on the kinetic theory of plasma. It was also emphasized by Longmire (1963), in chapter 4 of his seminal monograph, *Elementary Plasma Physics*.

6. The second generation of kinetic polar wind models

The second generation of exospheric polar wind models was developed by Lemaire and Scherer (1969, 1970, 1971, 1972). Instead of using a mono-kinetic velocity distribution function (VDF) for the H^+ ions at the exobase, they assumed a Maxwellian VDF with a truncated pitch angle distribution. The latter is piece-wise isotropic but partially depleted in the downward loss cone for particles coming in from infinity. Besides assuming no incoming particles, Lemaire and Scherer also defined escaping ones as those that have enough kinetic energy to overcome the total potential barrier between the exobase and infinity. Such particles can escape into the magnetotail and are considered to be lost for the topside polar ionosphere.

In Lemaire-Scherer's exospheric models there are also so-called ballistic particles, which are unable to escape and fall back into the collision dominating reservoir below the exobase. There are two extreme classes of exospheric models:

(i) those for which there are no trapped particles (i.e. ones with magnetic mirror points above the exobase), and (ii) those which are saturated with trapped particles in detailed balanced equilibrium with the ballistic ones. Of course, partially saturated trapped populations can also be considered; they all form the family of intermediate exospheric models that can be labeled "zero-order kinetic models" – higher-order kinetic models being those that take into account local collision between particles, as in the kinetic models based on the Fokker-Planck equation and discussed in Sect. 10. Naturally, in addition to local collisions and pitch angle scattering, future higher order kinetic models will also have to take into account non-local collisions, i.e. collisions experienced at high altitudes, several density scale heights from the exobase. Indeed, such distant collisions backscatter escaping and trapped particles into the downward loss cone and modify the VDF of incoming particles at lower exospheric levels. These non-local collisions could be taken into consideration by keeping the effects of collisions even when they are weak enough so that they take place over many density scale heights. This is included in different collisional models like those given by Barakat et al. (1990; 1995); Barghouthi et al. (1993); Demars et al. (1998); Pierrard and Lemaire (1998); Lie-Svendsen and Rees (1996); and Tam et al. (1995a). Adequate data to test these ideas is limited, however.

It should be pointed out here, that the exospheric description had been pioneered by Eviatar et al. (1964) to describe the density distribution of thermal protons and electrons of ionospheric origin that are trapped along *closed* dipole magnetic field lines. Kamiyama and Takaki (1966) extended this early ion-exospheric model by evaluating the effect resulting from the rotation of the magnetic dipole on the field-aligned plasma density distribution. A subsequent generalization of these early "zero-order kinetic protonosphere models" was elaborated by Hartle (1969, 1971). Hartle extended Eviatar et al.'s ion-exospheric model by allowing that the ion and electron densities and temperatures could be

different at conjugate exobase (or baropause) levels in both hemispheres. In all these early exospheric models the Pannekoek-Rosseland electric potential distribution was assumed to maintain the quasi-neutrality of the proton-electron plasma. A later application of exospheric theory to the problem of closed geomagnetic field lines was published by Huang and Birmingham (1992) who studied the effects of anisotropic rotating magnetospheric plasmas on the polarization electric field distribution along magnetic field lines. Reviews on exospheric theories of ionized and neutral planetary atmospheres including observational evidence were presented by Fahr and Shizgal (1983) and by Shizgal and Arkos (1996).

Note that in the (ideally collisionless) exospheric models, the effects of local and non-local collisions are completely neglected. The different classes of particles trajectories (i.e. trapped, ballistic, etc.) are distinct. In such cases, trapped and ballistic particles contribute to the exospheric density, pressure tensor, and all even moments of the VDF. They don't contribute to the odd moments of the VDF (flux, energy flux…). On the other hand, as the effects of collisions are introduced, the distinction between these classes becomes less sharp because a particle can become trapped/untrapped due to diffusion in the velocity space. Therefore, in the presence of collisions, it is not clear how to distinguish between classes of particles that contribute or not to the different odd moments (flux, heat flux, etc.).

Furthermore, in the second generation of PW exospheric models the temperatures characterizing the dispersion of velocities of the H^+ or He^+ ions at the exobase are free parameters. They can be chosen to be different for each ion species and for electrons. As noted above, and in Appendix B, the number and quality of polar wind observations that can be used to constrain PW models has been limited until recently.

Unlike in the first generation exospheric PW models, the electrons are also considered collisionless particles, and their VDF in the exosphere is a solution of Liouville's equation (or Vlasov equation), assuming an anisotropic (truncated) pitch angle distribution and a Maxwellian energy distribution at the exobase; a similar approximation was used to calculate the VDF of the O^+ ions in Lemaire-Scherer's polar wind exospheric models.

These solutions of the Liouville equation are assumed to be analytical functions of the gravitational potential, $\phi_g(r)$, as well as the to-be-determined electric potential, $\phi_E(r)$. The moments of these VDFs are analytical functions of these potentials, restricted by boundary conditions imposed at the altitude of the exobase. In the first generation exospheric models the electric potential, $\phi_E(r)$ was derived from the Pannekoek-Rosseland electric field, Eq. (A1). In the exospheric models of Lemaire-Scherer $\phi_E(r)$ is calculated by successive iterations under the restriction that the electron charge density ($e\, n_e$) is equal everywhere to the total ion charge density ($\Sigma_i\, Z_i\, e\, n_i$).

Furthermore, the total electric potential difference, $\phi_E(\infty) - \phi_E(r_{exobase})$, between the exobase and infinity is determined such that the net flux of electrons capable of escaping out of the electric potential well is balanced by the net Jeans flux of escaping ions. This condition can be and has been relaxed in subsequent exospheric models, where electric currents are allowed to flow along geomagnetic field lines as, for instance, in the auroral upward or return current regions. The zero-current condition (corresponding to the original PW models) leads, in general, to larger field-aligned electric potential differences than the Pannekoek-Rosseland electric field.

Observational constraints on field-aligned electric potential differences are scarce and indirect. Fung and Hoffman (1991) used photoelectron observations and a model to show no more than a 2-V potential drop between the altitudes of 400 and 900 km, corresponding to a distributed parallel dc electric field of less

than 4 microV/m on auroral field lines. Peterson et al. (1977) used spectral features in photoelectron spectra simultaneously observed from conjugate hemispheres to infer that the potential drop between hemispheres on closed field lines was less than 1.5 eV.

Once the electric potential is determined at all altitudes in the PW ion-exosphere, it is straightforward to use the analytical expressions for the moments of the VDFs to calculate the distributions of the ion and electron densities, their average or bulk velocity, the components of the kinetic pressure tensors, energy flux, and parallel or perpendicular temperatures at all other altitudes.

Also, once the value of ϕ_E, the electric potential, is known at an arbitrary number of discrete altitudes (r_l), the electric field distribution $E(r_l)$ can be obtained by numerical differentiation of $\phi_E(r)$: $E = - \nabla\phi_E$. As a test of the numerical codes, it has been verified that the values of electric field intensity calculated at these discrete altitudes are indeed consistent with the values derived from the gradient of the electron kinetic pressure, according to Eq. (2).

As a further test of the numerical code it was also verified, by computing the second-order derivative of the electric potential ($\nabla^2\phi_E$), that the electric charge density in the right-hand side of Poisson's equation is extremely small and that the quasi-neutrality condition is therefore satisfied to a very good approximation. The parallel component of the polarization electric field is assumed to be extremely small in the polar wind. It is generally smaller than 10^{-3} mV/m in the exospheric models of Lemaire and Scherer (1974a) as illustrated in Fig. 2. The solid line corresponds to the parallel electric field intensity in an exospheric model where incoming and trapped particles are missing from the H^+, O^+ and electron VDFs. The dotted curve corresponds to the Pannekoek-Rosseland electric field of the isothermal hydrostatic model. It is also called the barometric model. In this model the incoming particles and trapped particles are not missing, but in equilibrium with the ballistic and escaping ones at all altitudes; the VDF is Maxwellian and

isotropic. The dashed curve corresponds to the third extreme case where only the incoming particles are missing in the VDF. Note that the parallel electric field is smaller in the case of hydrostatic equilibrium than in the other two extreme exospheric models where the VDF is truncated and some classes of particles are missing. For intermediate classes of exospheric models with partially populated particle orbits, the charge separation electric field has intermediate values depending on the relative abundances of each class of particles forming the ion and electron VDFs.

When more warm electrons and ion populations from the magnetosphere (0.1-5 keV) are added to the cold ionospheric plasma (< 1 eV), as for instance in polar cusp flux tubes, an electrostatic double layer can be formed in the ion-exosphere at the altitude where the cold and warm electron densities become equal. Peak values of the electric field may then exceed 10^{-1} mV/m in a narrow region at or above 20,000 km altitude, as shown in the polar cusp models by Lemaire and Scherer (1978)*. This is illustrated in Fig. 3c and 3d where the parallel potential and electric field distributions are, respectively, shown versus altitude in a polar cusp flux tube containing both cold O^+ and H^+ ionospheric ions and electrons as well as warm magnetosheath protons and electrons. Fig. 3a and 3b respectively illustrate the field-aligned distributions of the number densities and bulk velocities of the cold and warm ions and electrons. At the altitude of about 20,000 km, where the electrostatic double layer is formed, the cold electron density drops to almost zero; the H^+ ion density also has a sharp drop, while their upward PW bulk velocity is drastically enhanced by the large double layer electric field intensity from less than 15 km/s up to 70 km/s

* A similar model calculation has been performed more recently for an auroral flux tube by Ergun et al. (2000), who found peak electric fields of 40 mV/m at a geocentric distance of about 2 Earth radii in their multi-ionic plasma simulations (see Fig. 4 in Ergun et al., 2000).

(Lemaire and Scherer, 1978).* Similar results were obtained by Barakat and Schunk (1984) using a semi-kinetic model in which the ions were treated as particles and the electrons were treated as a massless fluid.

Note also that the density scale height of the O^+ ions is 16 times smaller than that of the H^+ ions so that its density is already negligibly small at the altitude of the double layer. For different boundary conditions in the ionosphere and at high altitudes the double layer may form at lower altitudes where the O^+ is relatively larger than in this example. Under such circumstances a much larger number of the O^+ ions can be energized by the peak electric field and be injected into the magnetosphere.

7. Bi-Maxwellian velocity distribution functions

In all exospheric models discussed earlier it has been assumed that the energy spectrum or velocity distribution function of all particle species (O^+, H^+, He^+, e^- of ionospheric origin and p^+, e^- of magnetosheath or magnetospheric origin) are Maxwellians at the exobase or in their high altitude source region. A bi-Maxwellian VDF has been considered by Lemaire and Scherer (1971). Different parallel and perpendicular temperatures at the exobase complicate the mathematical expression of the moments of the VDF. However, it does not necessarily drastically change the spatial distributions of the ions and electrons densities along the geomagnetic field lines. As a consequence, this model generalization and sophistication does not significantly change the exospheric distributions of the field-aligned potential and electric field in polar wind models. When $T_{//} \neq T_{\perp}$ at the exobase, only the values of the higher-order moments of

* Note that the polarization electric field has a component parallel to magnetic field lines; this necessarily invalidates the condition $\mathbf{E}.\mathbf{B} = 0$ for the ideal MHD approximation to be applicable. This is also the necessary condition for magnetic field lines to be equipotential, and so to speak be "frozen-in" the plasma, unless it is the plasma that is "frozen-in" to the magnetic field line… it is not always obvious to know which is semantically more incorrect.

the VDF (i.e., the components of the kinetic pressure tensor, energy flux…) can then be more significantly altered in the ion-exosphere.

Asymmetric Maxwellian VDF with a non-zero displacement velocity, u_{H^+}, have also been tried at the exobase to determine the density and bulk velocities of H^+ and O^+ ions at the exobase (Lemaire and Scherer, 1972). The solid and dashed lines in Fig. 4 show the H^+ and O^+ ion densities in such asymmetric exospheric models, respectively, for $u_{H^+} = 0$ and for $u_{H^+} = 1.4$ km/s. The dotted lines show the corresponding densities for Banks and Holzer's (1969b) hydrodynamic model, for reference. The vertical bars at altitudes ~1200-1300 km correspond to the exobase level, where both exospheric models have been fitted to hydrodynamical models in the collision-dominated region of the polar wind. It can be seen that a displaced Maxwellian with $u_{H^+} \neq 0$ does not drastically alter the distributions of the O^+ and H^+ at some distance from the exobase levels. The same holds true for the bulk velocities, for they are slightly increased in the vicinity of the exobase when $u_{H^+} \neq 0$, but not at higher exospheric altitudes.

8. Lorentzian velocity distribution functions

A rather convenient way to enhance the suprathermal tail of a VDF is to adopt a Lorentzian function to describe the distribution of particle velocities

$$f(\mathrm{v}, r, t) = n(r,t)\left(1 + \frac{mv^2}{2\kappa kT}\right)^{-(\kappa+1)} \quad . \tag{3}$$

For small values of the velocity, v, the shape of this VDF tends to fit a Maxwellian with density, n, and temperature, T. However, for v significantly larger than the thermal speed $(kT/m)^{1/2}$, the distribution of the particles varies as a power law $(mv^2/2kT)^{-\kappa}$, instead of exponentially ($\exp(-mv2/kT)$), like for the Maxwellian VDF.

Power law energy spectra are commonly observed in nature (cosmic rays, Van Allen belt particles, plasmasheet particles, solar energetic particles, etc...). The

energy spectra for polar wind electrons and ions below 2 eV is not easy to measure with in-situ experiments, therefore there is no firm evidence that Lorentzian VDF might be more realistic than the usual Maxwellian VDF for suprathermal particles whose energies range from 0.5 eV to over 10 eV. Nevertheless, it is interesting from a theoretical point of view to predict what would be the effects of suprathermal tails in the velocity distribution function of escaping polar wind electrons. It has been found that increasing the hardness of the electron energy spectrum dramatically increases the flux of electrons that have sufficient energy to escape out of the electrostatic potential well; this increases the electrostatic potential difference between the exobase level and infinity. A third generation of exospheric models using a Lorentzian VDF at the exobase has been developed by Pierrard and Lemaire (1996).

The escape flux of the ionospheric electrons is thus enhanced when their VDF has a suprathermal tail, i.e. when the energy spectrum becomes harder and when the index κ in Eq. (3) is equal to 5 or 4 instead of ∞. Consequently, a larger field-aligned potential difference, $\phi_E(r_o) - \phi_E(\infty)$, is required for the net escape flux of electrons to remain equal to that of the polar wind H^+ ions, i.e. for the field-aligned current density to stay equal to zero. As a result of the larger field-aligned potential difference, the H^+ ions and He^+ ions are accelerated to higher supersonic polar wind bulk velocities. In other words, when the VDF of the PW electrons has an enhanced suprathermal tail or harder energy spectrum, the asymptotic bulk speed and flux of the polar wind H^+ ions is enhanced. The artifact of using a Lorentzian VDF instead a Maxwellian VDF significantly increases the flux of energy carried away from the ionosphere by the escaping electrons, as well as any higher order moments of the electron and ion VDFs. (See Sect. 9 and 10 for more discussion of the role of photoelectrons in polar wind theories.)

Polar wind modelers have not yet offered convincing physical justification regarding why the exobase VDF should not be Maxwellian, instead of Lorentzian. Several theoreticians have proposed various ways to enhance the population of suprathermal electrons in plasma (Collier, 1993; Collier and Hamilton, 1995; Summers and Thorne, 1992; Treumann, 1997). In addition to wave-particle interaction mechanisms often invoked when nothing else works or has been imagined, the presence of photoelectrons in the sunlit ionosphere is of course a well identified source of suprathermal electrons. For the polar wind it was indeed the first source invoked by Axford (1968) to drive the polar wind. The addition of sufficiently large fluxes of photoelectrons can indeed increase the flux of polar wind ions and their asymptotic bulk speed due to the larger field-aligned electric potential difference. However, Banks and Kockarts (1973) showed that the upward flux of photoelectrons (> 1 eV) is generally significantly smaller than the escape flux of the thermal electrons (< 1-2 eV). Consequently, the contribution of photoelectrons in "dragging the H^+ ions out of the polar ionosphere" was shown by Lemaire (1972b) to be rather marginal compared to the significantly larger escape flux of the thermal ionospheric electrons, even in the dayside local time sector. The effect of photoelectrons has now been reconsidered and discussed in more comprehensive modeling efforts by Barakat and Schunk (1984), Tam et al. (1995a,b), Khazanov et al. (1997a,b, 1998), and Barakat et al. (1998b). Their main contributions are summarized in the following sections.

9. Third generation of kinetic polar wind models and effects of photoelectrons

One decade after the effect of photoelectrons on the polar wind flow had been first pointed out, its influence on the field-aligned electric field was rediscovered based on the observed "anomalous" photoelectron distributions over the polar cap (Winningham and Gurgiolo, 1982). Another decade later, the effect of the photoelectrons driving the polar wind was inferred from the

observed day/night asymmetry in the outflow of thermal O^+ in the polar cap (e.g. Horita et al., 1993), and the availability of reliable measurements of thermal electron anisotropies (e.g. Yau et al., 1995) from the Akebono satellite. Photoelectrons quickly became a hot topic in theoretical polar wind studies. It was then re-emphasized that large fluxes of photoelectrons would be able to increase the electric potential difference between the exobase and the magnetosphere well above the standard value of 2-3 volts corresponding to the polar wind in absence of any photoelectron flux.

Increasing the electrostatic potential difference between the exobase and infinity lowers the critical escape velocity of the O^+ ions, reduces the altitude where their potential energy has a maximum, and it decreases the value of the potential barrier that the ions must overcome in order to escape to infinity.

The first and second generations of exospheric models were developed for cases where the field-aligned distribution of the total potential energy is either (i) a monotonically increasing function of altitude (for the electrons), or (ii) a monotonically decreasing function of height (for H^+ or He^+ ions). It was not developed for the case when the total potential energy has a maximum at a given altitude above the exobase. This is, for instance, the case for the O^+ ions. The presence of such a maximum in the field-aligned distribution of the total potential energy of the O^+ ions was noted by Lemaire and Scherer (1972) but it was not viewed as a key issue. Such a maximum adds a larger number of possible classes of particle orbits in the magnetic, gravitational and electrostatic fields. In their exospheric PW models where the total potential drop was less than 2 volts, this maximum occurs beyond 20,000 km where the O^+ ions density has become a negligibly minor constituent compared to the H^+ ions, in their polar wind model (see Fig. 1 in Lemaire and Scherer, 1972). Beyond such extreme altitudes in the exospheric models of Lemaire-Scherer, the O^+ density was set equal to a vanishingly small constant density, since at those altitudes n_{O+} has become a

negligible term in the quasi-neutrality equation, and therefore no longer affects the electric potential distribution. Unless the electrostatic potential difference between the ionosphere and the magnetosphere significantly exceeds 2-3 volts the effect on the exospheric distributions of H^+ and He^+ was presumed negligible.

Chiu and Schulz (1978) point out that, in principle, this was an inconsistency in the second generation of exospheric polar wind models where the potential energy of the O^+ ions is handled as a monotonically increasing function of altitude, and a monotonically decreasing function of height for the H^+ ions. Chiu and Schulz (1978) clearly posed the problem of "accessibility" of some classes of ballistic particles, and introduced the accessibility conditions:

$$d\,\phi_E / d\,B > 0 \tag{4}$$

$$d^2\,\phi_E / d\,B^2 \leq 0 \tag{5}$$

These constraints imply that the electrostatic potential must increase smoothly from the point of minimum B, with a smoothly decreasing gradient. These constraints fail to be satisfied in second generation exospheric models, especially when photoelectrons or magnetospheric populations co-exist in magnetic flux tubes with cold ionospheric particles. Although Chiu and Schulz (1978) correctly pointed out this deficiency, they did not however, propose any method to resolve this issue.

Barakat and Schunk (1983, 1984) investigated the effects of photoelectrons and elevated temperature of ambient electrons, using a semi-kinetic polar wind model. It was concluded that a non-monotonic potential barrier (for the O^+) forms. This necessitates the simultaneous solution of the coupled equations for a range of altitudes. They briefly outlined the new requirements and solved it in a self-consistent manner. It was found that the escape flux of O^+ was significantly influenced when the maximum O^+ potential occurred at altitudes less than or about 3 Earth radii.

Khazanov et al. (1997a,b) extended the number of classes of particle orbits in velocity space, and worked out extended analytical expressions for the moments of the VDF when the total potential energy is not a monotonically increasing function of height. They proposed also an iterative method to determine the field-aligned electric potential in cases when the conditions, Eq. (4) and Eq. (5), are not satisfied.

Since these accessibility conditions are sometimes violated in Lemaire-Scherer exospheric models, it was relevant to develop a more comprehensive formulation for more general exospheric models. Khazanov et al. (1998) presented general solutions to the Vlasov equation for free-flowing plasma along magnetic field lines using Liouville's theorem, allowing for an arbitrary potential structure including non-monotonicities violating Chiu and Schulz's generalized constraints.

Instead of the Chiu and Schulz's constraints imposed on ϕ_E by the inequalities of Eq. (4) and (5), the following new constraints were introduced by Khazanov et al. (1998) in their Appendix B:

$$d\ \Pi / d\ B \ \text{must be monotonic} \tag{6}$$

$$d^2\ \Pi / d\ B^2 > 0 \quad \text{if} \quad d\ \Pi / d\ B < 0 \tag{7}$$

where $\Pi(B)$ is a generalized potential energy:

$$\Pi = Ze\ \phi_E - m\ (\Psi_G + \Psi_{PM} + \Psi_C). \tag{8}$$

It takes into account respectively the gravitational potential, a tentative ponderomotive potential, and the centrifugal potential, Ψ_G , Ψ_{PM} and Ψ_C for each particle species of mass m and electric charge Ze (see Appendix A in Khazanov et al., 1998).

Note that these new constraints are on the derivatives of the potential energy with respect to the magnetic field intensity, not distance or altitude. The new analytical expressions for the moments of the VDF have been formulated in terms of Π for each individual PW particle species (H^+, O^+, e^-). The generalized

expressions for the densities, particle flux, pressure tensor components, and energy flux in this third generation of exospheric models have been derived by Khazanov et al. for different truncated VDF at the exobase – bi-Maxwellian and bi-Lorentzian functions. In their Appendix D, they also verified the corresponding moments used in the second generation models are recovered from these more general formulae when the accessibility constrains of Eq. (6) and (7) are not violated.

Three generalized model results (dashed lines) are compared in Fig. 5 with those of a semi-kinetic polar wind model (solid lines) calculated by Khazanov et al. (1997a), which belong to the category of the second generation exospheric models. Three different values of photoelectron content are assumed at the base of the model (500 km): n_{po} = 0.01 %, 0.03 %, 0.05 %. N_{po} is the fraction of electron density at 500 km accounted for by photoelectrons with 20 eV characteristic energy. Fig. 5 illustrates the field-aligned distributions of (a) the total potential difference (electrostatic and gravitational) for O^+, (b) the O^+ density, and (c) the thermal electron temperature. It can be seen that the total potential energy distribution for O^+ changes substantially between the two models for higher levels of $n_{po.}$. In fact, the result changes from a net deceleration to a net acceleration of O^+. This difference is mainly due to the fact that the new model introduces a "hole" in the O^+ velocity distribution function at high altitudes, above the altitude of the maximum potential barrier.

In the previous model of Khazanov et al. (1997a,b), this "hole" was filled with particles having a Maxwellian VDF, causing the calculation to converge to a different potential energy distribution above the peak barrier. Due to the dependence of the solution at a given spatial point on its values above and below this location, the iteration process yields different results for the two models along the entire field line for higher photoelectron concentrations. This change in the potential energy curves has the effect of increasing the density of O^+ by orders of

magnitude in the high-altitude region. Also shown is the thermal electron temperature in both models. The same energy equation was used in both models, yet the electron temperature, T_e, is increased in the new third generation PW model due to the change in the distribution of the total potential energy along the field line (see Fig. 5a).

Khazanov et al. (1998) also showed that the photoelectron-driven polar wind outflows is not significantly different from the second generation exospheric models for low and moderate values of the photoelectron content ($n_{po} < 0.03$ %,). This fails to be true for higher photoelectron concentrations ($n_{po} > 0.05$ %).

The effect of hot magnetospheric or polar rain electrons on the PW was also studied by Barakat and Schunk (1984) by including in their model calculations precipitating hot electrons of magnetospheric origin in the polar cap region. But their approach only treats the ions kinetically, while it treats the electrons as a massless fluid. The effect of sudden impulses in the electron temperature on the polar wind has been examined by Ho et al. (1991) based on a semi-kinetic approach. The effects of magnetospheric electrons on polar plasma outflow has been modeled by Ho et al. (1992) using this same type of approach. The effects of centrifugal acceleration on the polar wind have been considered by Horwitz et al. (1994). The tutorials by Schunk (1986, 1988) and a more recent review by Ganguli (1996) provide quite a complete picture of the historical development of these types of polar wind models.

10. Fourth generation of kinetic polar wind models

In all previous kinetic models the exobase surface was assumed to be a sharp discontinuity where the collision frequency jumps from a finite value to almost zero; at the exobase the mean-free-paths of all upward moving particles are assumed to become arbitrarily large. In reality however, the change from a

collision dominated flow regime to a collisionless one occurs over a transition region, which has a thickness of several density scale heights, H.

In post-exospheric kinetic models the gradual change of the VDF across this exobase transition region is determined by solving the Boltzmann equation in the case of neutral atoms for which binary collisions are most important, or by solving the Fokker-Planck equation in the case of ions and electrons when long-range Coulomb interactions are most important to scatter and diffuse particles. The vector A is the so-called "dynamic friction" and D is the "velocity diffusion tensor as defined in Spitzer (1956) or Hinton (1983). Under steady state conditions and assuming that the plasma is not moving in a horizontal direction the Fokker-Planck equation is given by:

$$v.\frac{\partial f}{\partial \vec{r}} + \frac{\vec{F}}{m}.\frac{\partial f}{\partial \vec{v}} = -\frac{\partial}{\partial \vec{v}}\left[\vec{A}f - \frac{1}{2}\frac{\partial}{\partial \vec{v}}.(Df)\right] \qquad (9)$$

where it is implicitly assumed that the guiding centers of the ions and electrons move independently along the geomagnetic field lines (assumed to be those of a dipole). It is this latter equation that has been solved independently by Lie-Svendsen and Rees (1996) as well as by Pierrard (1997) to calculate the VDF in the transition region of the polar wind. This partial differential equation (PDE) can be solved by using different mathematical and numerical methods. Pierrard (1997) solved this equation by using a novel powerful spectral method: i.e. by expanding the VDF in a series of orthogonal polynomials of the velocity, v (speed polynomials), of the pitch angle, θ (Legendre polynomials in $\mu = \cos\theta$) and of the radial distance, r (Legendre polynomials). These results will be discussed below. On the other hand, Lie-Svendsen and Rees (1996) adopted a standard finite difference method with fixed and time-independent boundary conditions at the bottom and top of the transition region. Their results are illustrated in the left hand panels of Fig. 6.

In Fig. 6, the iso-contours of meridional cross-sections of the VDF are shown for three different altitudes in the transition region. The bottom panel illustrates the low altitude boundary conditions used by these authors to solve the Fokker-Planck equation. For all upward directed velocity (i.e. for $\mu = \cos\theta > 0$) they assumed a Maxwellian and isotropic VDF in the upper half hemisphere of the velocity space. The velocity and pitch angle distribution for $\mu < 0$ is determined by the boundary condition at the top of the transition region where they assumed that there were no particles with downward directed velocities larger than the critical escape speed. It is clearly seen that the pitch angle distribution changes from an almost isotropic one (with a peak at $\mathbf{v} = 0$ in velocity space) to a doubly peaked VDF with a secondary bean shaped maximum. This peak occurs at a velocity that increases with the altitude in the transition region like the bulk velocity in the hydrodynamic PW models (see Fig. 1).

This secondary peak which becomes predominant at high altitudes is formed by particles with velocities larger than the thermal velocity of the H^+ ions. Note that it is these suprathermal particles that contribute most to the net upward polar wind flux, and it is also these suprathermal particles that contribute most effectively to all odd moments of the VDF. This is just like in exospheric models where the net flux of particles and energy is only carried by the escaping particles, and not by the ballistic or trapped particles.

The peak at the origin in velocity space corresponds to ballistic particles in exospheric models; they have an isotropic pitch angle distribution. All of these sub-thermal velocities have a nearly Maxwellian and isotropic VDF in the vicinity of $\mathbf{v} = 0$. Indeed, due to the v^{-4} dependence of the Coulomb collision cross-section, these sub-thermal particles have a large collision frequency. Therefore, they tend to thermalize/Maxwellize more quickly than the suprathermal ones; their VDF relaxes more rapidly toward an isotropic Maxwellian than the more energetic ones, as a consequence of the velocity dependence of Coulomb

collisions. This is at the source of the isotropic Maxwellian peak in the VDF at **v** = 0, and illustrated in the left-hand side panels of Fig. 6.

Just like in the case of hydrostatic equilibrium the component of **u** parallel to the magnetic field line is equal to zero. This is not the case, however, for the VDFs implicitly postulated in hydrodynamic models of the polar wind, as illustrated in the right-hand side panels of Fig. 6. Indeed, in such hydrodynamic models the VDFs have a peak at **v = u,** where **u** is the bulk velocity and also the displacement velocity of the zero order approximation of the VDF in the Chapman-Enskog's theory (see Sect. 13). The vestigial Maxwellian peak of the Fokker-Planck solution centered around **v** = 0 may be regarded a population of collision dominated particles. Their VDF is symmetric, therefore they don't contribute to the escape flux nor to the mean bulk speed, **u**, unlike in hydrodynamic models. Only the particles moving upward with a suprathermal velocity, and exceeding the critical escape speed contribute to the escape flux, and therefore to the mean polar wind bulk velocity, **u**, in Fokker-Planck kinetic models of the polar wind.

Note also that for $\mu = \cos\theta = 0$ – i.e. for the particles moving in any horizontal direction – the VDF should be Maxwellian over the whole range of energies. In all horizontal directions the density is uniform in the transition region, therefore Coulomb collisions tend to produce a Maxwellian distribution for all particles moving in horizontal directions; the steady state equilibrium VDF in a uniform gas/plasma is indeed a Maxwellian.

Pierrard (1997) pointed out that the VDF must satisfy boundary conditions at the bottom and at the top of the transition region that are necessarily restricted by two regularity conditions: (i) the VDF has to be isotropic in the limit **v** = 0; and (ii) the VDF has to be Maxwellian in the limit $\mu = \cos\theta = 0$.

These regularity conditions were first introduced and applied in kinetic polar wind models by Pierrard (1997) and Pierrard and Lemaire (1998). These regularity

conditions were not applied at the bottom of the transition region in Lie-Svendsen and Rees (1996) model calculations.

The three panels in Fig. 7 illustrate the VDF at three different altitudes in the transition region. They have been obtained by using a powerful spectral method to solve Eq. (9) for the PW. The solution of this Fokker-Planck equation is based on a polynomial expansion of the VDF into three sets of orthogonal functions: (i) Legendre polynomials for μ (: cos θ), (ii) speed polynomials (Shizgal and Blackmore, 1984) for v, the velocities of the H^+ ions, and (iii) Legendre polynomials for r, the radial distance. It should be emphasized that this polynomial expansion has nothing in common with the well known classical expansion of the VDF in the Chapman-Enskog or Grad theories of non-uniform gases. Indeed, in the study of Pierrard-Lemaire, the zero-order solution is not forced to coincide with a displaced Maxwellian or bi-Maxwellian VDF as in the theory of Chapman-Enskog and of Grad. The solution illustrated in Fig. 7 is the result of polynomial expansions of order 10 in μ= cos θ (Legendre polynomials), of order 10 in v (speed polynomials), and order 10 in altitude (Legendre polynomials).

Note that only the VDF of the H^+ ions has been calculated. The density distributions of the O^+ ions and electrons were given as a function of the altitude in the transition region. These particles were assumed to be the dominant species and their VDF was assumed to be isotropic and Maxwellian in the whole transition region. This simplifying assumption is of course a convenient first step that can be relaxed, but not without significantly increasing the computational difficulties. That is why in the first attempts to solve the PW Fokker-Planck equation, Pierrard-Lemaire and Lie-Svendsen-Rees ignore self-collisions among the H^+ ions; this implies that the O^+ ions are the major ions in the whole transition layer and that their bulk speed remains small compared to the thermal speed of the minor H^+ ions. These difficulties have been overcome in the

macroscopic particle-in-cell models (e.g. Demars et al., 1998, 1999; Barakat and Schunk, 2001; and Barakat et al., 2003) and in the hybrid models of Tam et al. (1995a, 1995b, 1998) as demonstrated in Sect. 11.

The results obtained by the spectral method of Pierrard (1997) and shown in Fig. 7 are qualitatively similar to those obtained by the finite difference numerical method used by Lie-Svendsen and Rees and are shown in the left-hand side panels of Fig. 6. They are also similar to the results of Barakat et al. (1995). Indeed, despite a slightly different choice of boundary conditions, both models clearly indicate that the VDF of the polar wind H^+ ions gradually changes from a dominantly Maxwellian with a single vestigial peak at the origin in velocity space, to a doubly peaked VDF with a secondary maximum at a suprathermal velocity corresponding to a population of particles that have enough energy to be essentially collisionless with the O^+ background. These are again the particles that contribute mainly to the net escape flux of particles, mass and total energy in the topside polar ionosphere. Also note that the relative importance of both peaks change with the altitude in the transition region; the primary maximum that is dominant at the bottom, where Coulomb collisions are dominant, gradually fades away at higher altitudes where the secondary peak takes over, and becomes more and more prominent in the collisionless exosphere. This characteristic behavior of the H^+ VDF was also found by Barghouthi et al. (1993) and Barakat et al. (1995) using a Direct Monte Carlo Simulation (DMCS), as illustrated in Fig. 8.

Fig. 8 shows that the evolution of the VDF across the transition region predicted by all the different kinds of kinetic approaches and simulations converge toward a unified picture that is quite in contrast with that proposed in the hydrodynamic models. Indeed, the transformation of the VDF between the bottom and the top of the transition layer is basically different from that inferred from hydrodynamic/fluid polar wind models, like that illustrated in the right-hand side panel of Fig. 6. In those fluid approaches the VDF of the H^+ ions are

implicitly postulated to be a singly peaked function whose maximum is approximately to a displaced Maxwellian function with a displacement velocity, **u,** which is equal to the average velocity of the individual polar wind H^+ ions. The value of u is increasing continuously with the altitude from a subsonic value at the bottom to a supersonic one at the top of the transition layer.

This is a far reaching and basic difference illustrating how different the kinetic solutions for the VDF are from those postulated in the classical hydrodynamic theories of non-uniform gases developed by Chapman-Enskog or by Grad. It is clear that the latter do not correctly represent and simulate the kinetic outflow resulting from the evaporation of suprathermal particles out of a planetary gravitational potential.

11. Fifth generation of kinetic polar wind models

In previously described models the solutions of Eq. (9), the Fokker-Planck collisional operator was linear in the VDF of the H^+ ions because of the "test-particle assumption" and self-collisions of H^+ are neglected. However, observations (e.g., Abe et al., 1993, 2003) have indicated that the O^+ velocity can be significant in the daytime polar wind and the O^+ concentration is not negligible even at altitudes as high as 11,000 km. Therefore, for the daytime polar wind the O^+ population may be driven efficiently by the enhanced polarization (ambipolar) electric field due to the photoelectrons. In addition, the Fokker-Planck collisional operator must include the nonlinear interactions among the major and minor ions, including both cross- and self-collisions. Such a calculation has been performed by Tam et al. (1995a, 1998) based on a self-consistent hybrid model.

The model used an iterative Monte Carlo procedure to evaluate the Fokker-Planck collisional operator while following the kinetic evolution of the distributions of the O^+ and H^+ species, and the photoelectrons under the influence of a polarization electric field. Each iterative step was similar to the method used in Yasseen et al. (1989) and Tam et al. (1995b). The model was

hybrid in that its kinetic calculations were complemented by a set of fluid equations that determined the profiles of the polarization electric field, the thermal electron density, velocity and temperature. Solutions were obtained by iterations between the kinetic and fluid calculations until convergence.

Except for the case of the photoelectrons, which were treated as test particles in terms of collisions, the iterative scheme enabled the model to take into account the nonlinear effect of the Fokker-Planck collisional operator involving the self-collisions and cross-collisions of the ion species. Convergence of the results also ensured the self-consistency of the solution, including the polarization electric field, the density, velocity and temperature profiles of all the species, as well as the O^+, H^+, and photoelectron distributions.

This self-consistent hybrid model has generated results that agree with various observed polar wind features. For example, the theoretical calculations found that the total electron heat flux in the presence of photoelectrons was upwardly directed, in agreement with the dayside polar wind observation by the Akebono satellite (Tam et al., 1995a, 1998; Yau et al., 1995. Such an upward electron heat flux was also shown to be related to an enhancement in the self-consistent polarization (ambipolar) electric field, leading to an electrical potential difference that ranged up to a few volts, depending on the photoelectron concentration in the polar ionosphere (Tam et al., 1998). This result was consistent with the Dynamics Explorer (DE) satellite observations by Winningham and Gurgiolo (1982), who found that the potential difference varied over a similar range and depended on the solar zenith angle.

The enhancement of the self-consistent electric field due to the photoelectrons also addressed two dramatic effects on the polar wind ions observed by the Akebono satellite. First, the O^+ ions, instead of gravitationally bound, were driven to high altitudes by the self-consistent polarization electric field, maintaining their dominance over the H^+ ions (Barakat and Schunk, 1984;

Tam et al., 1995a, 1998; and Barakat et al., 1998a). The dominance by the O^+ species was observed even at high altitudes by the Akebono satellite (Abe et al., 1993, 2003). Second, the ions were more efficiently driven by the enhanced electric field. The presence (absence) of photoelectrons in the dayside (nightside) polar outflow thus led to an asymmetry in the ion outflow velocities between the day and night sectors, as demonstrated by Tam et al. (1998) and observed by Abe et al. (1993, 2003). The same result is obtained when the electron temperature is elevated in the dayside to higher values than in the nightside local time sector (Schunk and Sojka, 1997).

The theory of the photoelectron-driven polar wind (Tam et al., 1998) also addressed an observed asymmetry in the electron distribution. The presence of photoelectrons on the dayside, due to their upward heat fluxes, contributed to an anisotropy between the upwardly and downwardly moving electrons, where the parallel temperature for the former population was significantly higher. On the nightside, where photoelectrons were absent, no such anisotropy was found in the calculations. These results based on the theory of the photoelectron-driven polar wind are in agreement with the observations by the Akebono satellite (Yau et al., 1995; Abe et al., 1993, 2003).

12. Transport equations for modeling the polar wind

Numerous mathematical approaches have been used over the years to describe the polar wind and related flows, including the hydrodynamic, hydromagnetic, generalized transport, kinetic, semi-kinetic, Monte-Carlo, and particle-in-cell (PIC) techniques. It is useful to briefly describe them here.

The hydrodynamic, hydromagnetic, and generalized transport equations are obtained by taking velocity moments of the Boltzmann equation in order to obtain a system of transport equations for the physically significant moments of the distribution function, such as density, average or drift velocity, temperature,

stress tensor, heat flow vector, etc. Unfortunately, the transport equations do not constitute a closed system, because the equation governing the moment of order *r* contain the moment of order *r+1*. Therefore, to close the system of transport equations, it is necessary to adopt an appropriate expression for the velocity distribution function. If a pure Maxwellian is adopted, the simple Euler (5-moment) equations result (cf. Schunk, 1975, 1977). In this approximation heat flow and stress are neglected, and the properties of the plasma are completely determined by the density, drift or average velocity, and temperature. Chapman and Enskog extend the system of transport equations beyond the Euler approximation by expanding the velocity distribution function in an orthogonal polynomial series about a local Maxwellian which is characterized by the mean mass flow and average temperature of the gas mixture. In reality the expansion was done using the mean-free-path and, hence, the Chapman-Enskog equations only apply to collision-dominated plasmas. With this approach the density, average velocity, and temperature are the fundamental moments, while the stress, and heat flow moments are expressed in terms of the lower-order moments and their derivatives. This set of transport equations is also known as the Navier-Stokes system of transport equations. Note the Euler and Navier-Stokes system of transport equations are the classical hydrodynamic (or fluid) equations, which are only valid for collision-dominated plasmas.

As an alternate to the Chapman-Enskog approach, Grad (1949, 1958) expanded the velocity distribution function of each species in separate series expansions about individual local Maxwellians. Furthermore, Grad treated all velocity moments up to a certain order on an equal footing and thereby obtained a transport equation for each velocity moment. Depending on the level where the Maxwellian-based series expansion is truncated, one obtained the 5-moment, 13-moment, or the 20-moment approximations. Since the Grad expansion is not a mean-free-path expansion, Grad's transport equations can describe collisionless

as well as collision-dominated flows. It is worthwhile to emphasize that Grad's transport equations are not the hydrodynamic equations. In fact, when the 13-moment transport equations are expanded in a series with respect to the mean-free-path, the result is the Navier-Stokes system of equations (cf. Schunk, 1977).

For plasmas subjected to strong magnetic fields, the bi-Maxwellian velocity distribution function was introduced, which allowed for different temperatures parallel and perpendicular to the magnetic field in addition to the density and average velocity moments (6-moment approximation). The 6-moment transport equations were introduced by Chew et al. (1956), and subsequently, the bi-Maxwellian velocity distribution function was used as a zeroth-order term in a series expansion, which resulted in the 16-moment system of transport equations (Oraevskii et al., 1968; Chodura and Pohl, 1971; Demars and Schunk, 1979). This latter system of transport equations can be applied to both collision-dominated and collisionless plasma, and provides for a continuous transition between the regimes (see review by Barakat and Schunk, 1982a). Also, the bi-Maxwellian-based transport equations can describe non-Maxwellian plasmas, with temperature anisotropies as large as a factor of 20, and with large asymmetries along the magnetic field (Barakat and Schunk, 1982b). In the latter case, the peak of the velocity distribution does not coincide with the location of the average velocity.

The Maxwellian 13-moment and 20-moment transport equations and the bi-Maxwellian 6-moment and 16-moment equations are known as generalized transport equations. The hydromagnetic equations are the generalized transport equations without collision terms. The Monte-Carlo and particle-in-cell (PIC) techniques are based on following the motion of individual particles subjected to various forces and collisional processes (Barakat and Schunk, 1982c). A significant effort has been devoted to all the different approaches to modeling the polar

wind, but they are beyond the scope of this review which is mainly limited to kinetic modeling.

There are numerical problems with the various systems of transport equations since they form a system of stiff[♦] differential equations. Another difficulty arises from the presence of singular points in the system of partial differential equations. The number and various types of singular points depend on the approximation or closure scheme used to limit the series of generalized transport equations. The best known singularity is the sonic point, where the bulk velocity equals the sound speed in the supersonic polar wind model. The existence of these mathematical singularities leads to a numerical difficulty in obtaining steady state solutions of the coupled non-linear differential equations. Fortunately, in time-dependent flows this difficulty can be overcome (Mitchell and Palmadesso, 1983; Schunk and Watkins, 1981, 1982; Gombosi et al., 1985; Zinin et al., 1985; Singh and Schunk, 1985; Gombosi and Nagy, 1989; Wilson et al., 1990; and others)

An overview of the different contributions to polar wind modeling based on hydrodynamic and generalized transport equations can be found in Sect. 2.3 of the review by Ganguli (1996).

13. Comparison of kinetic and generalized transport models

With kinetic models, it is necessary to choose an expression for the velocity distribution function at the exobase. However, in the collisionless (or near collisionless) regime, it is not always obvious what the actual distribution function looks like. Therefore, over the years, several expressions have been adopted, including mono-energetic distributions, a truncated Maxwellian, a drifting or

♦ As per MATLAP News and Notes, March 2003 – An ordinary differential equation problem is stiff if the solution being sought is varying slowly, but there are nearby solutions that vary rapidly, so the numerical method must take small steps to obtain satisfactory results.

displaced Maxwellian, a truncated bi-Maxwellian, a drifting or displaced bi-Maxwellian, Lorentzian, and a bi-Lorentzian.

This zeroth-order velocity distribution is characterized by parameters which correspond respectively to the actual local density, n(r), drift or average velocity, u(r), parallel and perpendicular temperatures, and which are functions of the altitude along a flux tube. These lowest moments of the zeroth-order velocity distribution function are identical to those of the actual velocity distribution function. In the framework of the so-called 16-moment approximation, the field-aligned distribution of lower order moments of the velocity distribution function, as well as the additional higher order ones, are solutions of the closed set of 16 differential equations that provide the self-consistent model description.

It is expected, of course, that even higher order approximations of the generalized transport equations would give an even more accurate description of the actual velocity distribution function versus altitude as well as its appropriate moments. However, this improved higher order model description requires a larger number of boundary conditions at the exobase which are not usually available from observations.

Typically, the choice of the exobase velocity distribution functions was based on an educated guess of what one might suspect the distribution should look like. Yet, a rigorous mathematical approach is to expand the velocity distribution function in terms of an orthogonal polynomial series about some zero-order distribution function, where any one of the above mentioned distribution functions can be selected as the zeroth-order distribution function. This mathematical approach is exactly what is done to obtain generalized transport equations. However, if a series expansion is chosen for the velocity distribution function at the exobase, it would be necessary to have boundary conditions for all of the relevant velocity moments (density, drift or average velocity, parallel and perpendicular temperatures, parallel and perpendicular heat flow, etc.) at the

exobase, which is generally not possible. Nevertheless, this difficulty was overcome by Demars and Schunk (1991, 1992) in polar wind and solar wind studies.

Demars and Schunk (1991, 1992) compared the semi-kinetic and generalized transport methods for the case of steady-state polar wind outflow. For their generalized transport model, they used the 16-moment equations. As indicated earlier, the 16-moment transport equations are derived by taking velocity moments of Boltzmann's equation assuming that the zeroth-order velocity distribution function is bi-Maxwellian.

The semi-kinetic model used by Demars and Schunk (1991, 1992) is similar to that used by Holzer et al. (1971) in that it provides a description of the polar wind ions while the electron behavior enters the model through the form chosen for the polarization electric field. However, the semi-kinetic model used by Demars and Schunk (1991, 1992) differs from that of Holzer et al. (1971) in ways that allow for the most consistent comparison with the 16-moment transport equation. For example, the ion velocity distribution function at the exobase was assumed to be a bi-Maxwellian based 16-moment expansion with zero stress. Also, rather than using a simple Boltzmann relation to obtain the electrostatic potential energy, Demars and Schunk (1991, 1992) derived the electrostatic potential directly from the polarization electric field structure implicit in the 16-moment equations.

For the case of steady-state, supersonic, polar wind outflow, the 16-moment generalized transport equations were solved over an altitude range that extended from collision-dominated domain, through the transition region, and into the collisionless domain. The altitude where collisions became negligible was selected as the exobase and this is where the semi-kinetic solution began. A 16-moment velocity distribution function was adopted at the exobase and the boundary values for the parameters in the 16-moment function were provided by the solution of

the generalized transport equations. Subsequently, the kinetic expressions were used to determine the field-aligned exospheric distributions of all moments of the truncated ion velocity distribution function.

Fig. 9 shows the comparison of the semi-kinetic and generalized transport equations. It is apparent that the two solutions are nearly identical, even for the higher-order moments (parallel and perpendicular heat flows). These results indicate that the kinetic and generalized transport approaches are equivalent when the same velocity distribution functions are used in both approaches and when consistent boundary conditions are adopted at the top of the collision-dominated region or at the bottom of the collisionless one.

This good agreement between the solutions of the generalized transport equations and of the semi-kinetic or exospheric models is expected because all the moments of exospheric velocity distribution satisfy the whole hierarchy of moment equations up to any order of approximation, provided collisions can be ignored. Since the terms involving collisions in the generalized 16-moment transport equations are nearly negligible above the exobase, and since the ion velocity distribution function adopted at the exobase for the semi-kinetic model was identical to that provided by the solution of the generalized transport equations at the exobase altitude, both approaches are indeed expected to lead to the same field-aligned distributions for all 16 lower order moments. There is no such an agreement for the higher order moments beyond the heat flows ones. This satisfactory agreement between the semi-kinetic and generalized transport results indicates therefore that higher-order terms neglected in the 16-moment approximations will not significantly affect the field-aligned distribution of the lower order moments up to the heat flow ones provided, of course, consistent boundary conditions are used at the base of the exosphere.

It should, however, be pointed out that the steady state 16-moment transport equations are non-linear differential equations possessing a number of singular

points in the altitude range between the collision-dominated and collisionless regions – similar to the sonic transition point (Yasseen and Retterer, 1991). Unfortunately, these mathematical singularities constitute formidable numerical obstacles that can only be avoided, by directly solving the Boltzmann, Vlasov or Fokker-Planck kinetic equations, as outlined in Appendix B.

14. Monte-Carlo and PIC polar wind simulations

Using the macroscopic particle-in-cell (PIC) model developed by Barakat et al. (1998b), Demars et al. (1996a, 1996b, 1998) have studied several features of the polar wind. These studies simulate the plasma dynamics in a flux tube as it traverses the various regions of the high-latitude ionosphere, including the sub-auroral ionosphere, the dayside and nightside cusps, and the polar cap. The flux-tube trajectory and the lower boundary (2000 km) conditions adopted in these studies were based on results obtained from a three-dimensional, time-dependent, fluid model of the global ionosphere and polar wind (Schunk and Sojka, 1989, 1997). Demars et al. (1996a) found that the forward and reverse shock pairs were created in the plasma as the flux tube convected across regions of high electron temperature, namely, the dayside and nightside cusps. These shocks propagated upward and out of the simulation region. Demars et al. (1996b) used a PIC model to study the effect of centrifugal acceleration on the polar wind. It was found that the centrifugal acceleration does not significantly contribute to the loss of plasma from the polar ionosphere. Demars et al. (1998) studied the effect of trapped particles on the polar wind. They found that O^+ trapping is important and acts to increase the O^+ density at high altitudes.

Demars et al. (1999) compared fluid and PIC solutions for the time-dependent polar wind for a variety of realistic flux-tube trajectories, with both the trajectories and the PIC boundary conditions supplied by the model of Schunk and Sojka (1989, 1997). It was found that the fluid and PIC models are in

excellent agreement at lower altitudes (below 3000 km), but the solutions diverge at higher altitudes. This divergence is partly due to the inability of the fluid formulation to account for adiabatic kinetic processes, such as trapping, that occur at higher altitudes. Limitations of the PIC model also contribute to this divergence since, because of the small O^+ scale height, the number of O^+ simulation particles present at high altitudes was sometimes not sufficient to compute reliable densities.

15. Merits and limitations of kinetic polar wind models

Despite the rather crude assumptions on which they are based, exospheric and semi-kinetic models of the polar wind should not be disregarded and treated as "just academic exercises", as some considered them in the 1960's and thereafter. Indeed, when the proper field-aligned electric potential distribution is adopted, instead of the inappropriate Pannekoek-Rosseland electrostatic potential distribution, rather realistic values for the supersonic expansion velocities are obtained for the solar wind even with the simplest of these kinetic models.

The unchallenged merit is that it demonstrates how a polarization E-field is set-up within the plasma by the gravitational force, by the magnetic mirror effect, and by thermoelectric effects (Parks, 2004; and Appendix A). It shows how this internal E-field which has a component parallel to the magnetic field direction accelerates the ions to supersonic velocities along open magnetic field lines. It is the acceleration by this polarization electric field – hidden in the single fluid hydrodynamic momentum equation – that drives the solar wind and polar wind H^+ and He+ ions to supersonic velocities. The hydrodynamic analogy with Bernoulli's flow in a deLaval nozzle that was originally put forward by Parker (1963) to "explain" how the collisionless solar wind becomes supersonic may be viewed as an illustration, but by no means proof of what is really accelerating the collisionless solar wind and polar wind plasmas to supersonic speeds. This sort of

analogy is misleading since the deLaval noozle acceleration applies as well to gas of neutral atoms or molecules, while the acceleration of solar wind and polar wind particles would not occur if these particles would not be electrically charged.

Besides this important feature of exospheric models, their main acknowledged limitation is that collisions are fully neglected above some exobase altitude; furthermore that this exobase actually depends on the energy and pitch angle of the particles. The Knudsen number for sub-thermal ions is much smaller than that for the more energetic suprathermal ions. In addition, their mean-free-path depends on the pitch angle between their velocity and the direction of the magnetic field. This implies that the concept of a single exobase as a sharp surface of discontinuity between the collision dominated regime and the collisionless one is not more than a crude approximation. More realistic solutions should continue to be developed and more sophisticated polar wind models such as the collisional mac-PIC (macroscopic particle-in-cell) and post-Fokker-Planck models.

It is important to note that, at the time the first PW models were proposed, the state-of-the-art in thermal plasma measurements was not sufficiently developed to provide direct measurements of the velocity distribution function polar wind ions and electrons to guide the modelers. Only the lower order moments of the VDF (the density and particle flux) could be deduced from the measurements, thus a simple hydrodynamic model seemed to be sufficient, while a kinetic description was beyond the grasp of the experimental data available. Therefore, the development of polar wind theory and models has not been as intensively explored as, for instance models for radiation belt fluxes, because of the scarcity of relevant ion observations at energies below 1 eV.

A short history of polar wind observations is given in Appendix B. The synoptic recent data sets acquired by the Akebono and Polar satellites will be reviewed by Yau et al. (2006) in this issue.

Appendix A: The polarization electric field

The energy needed for a singly charged ion to escape out of the gravitational potential is smaller than for the corresponding neutral atoms. This is due to the electric potential difference induced in the ionosphere by the gravitational charge separation between the electrons and heavy ions. The polarization/ambipolar electric field produced by this kinetic mechanism of gravitational charge separation was first introduced in the study of ionized stellar atmospheres by Pannekoek (1922) and Rosseland (1924). They showed that when a fully or partially ionized atmosphere is in hydrostatic equilibrium within the gravitational field, $\boldsymbol{g}$, a polarization electric field is produced and is equal to

$$\boldsymbol{E} = - \mu \boldsymbol{g} / e \qquad \text{(A1)}$$

where $|e|$ is the charge of an electron and μ is a mean ionic mass defined by

$$\mu = (m_i^+ - m^-) / 2 \qquad \text{(A2)}$$

m_i^+ is the mass of the singly charged ions (Z_i=+1), m^- the mass of the electron (Z_e=-1). Eq. (A2) is applicable only when the ion temperature, T_i^+, is equal to the electron temperature, T_e^- (Mange, 1960, 1972; Bauer, 1966). Lemaire and Scherer (1970, Eq. A3) showed that in an isothermal multi-species plasma with multi-charged ions ($Z_i \neq +1$), the expression for μ becomes:

$$\mu = (\Sigma_j Z_j m_j n_j/T_j)/(\Sigma_j Z_j^2 n_j/T_j) \qquad \text{(A3)}$$

This expression is applicable even when the electron temperature is not equal to that of the different ion species: i.e. when $T_i^+ \neq T^+_{i+1} \neq T_e$. The sum is extended over all the charged species (ions and electrons). A derivation of this expression for the Pannekoek-Rosseland electric field is also given in Sect. 5.2.2 of the book by Lemaire and Gringauz (1968).

Since the electric force, $Z_i e \mathbf{E}$, on positive ions is directed upwards, in the opposite direction of the gravitational force, $m_i \mathbf{g}$, the effective total force on positive ions is reduced and can even be upward directed for the light ions (H^+,

He^+) in the polar cap ionosphere where O^+ ions are more abundant than the H^+ ions.

It is this Pannekoek-Rosseland electric field that Dessler et al. (1968) invoked to accelerate the H^+ ions to large (supersonic) bulk speeds in their polar breeze model. Thus, this polar breeze has been the very first exospheric and kinetic model of the polar wind.

When the plasma is not isothermal – i.e. when $\nabla T_j \neq 0$ – there is no simple algebraic relation between the polarization electric field intensity and the gravitational acceleration, even when the plasma is in hydrostatic equilibrium. If in addition, the plasma is not in hydrostatic equilibrium (but expanding as for instance in the solar wind and polar wind) the polarization electric intensity can not be derived from a simple algebraic expression like Eq. (A1); additional terms have to then be included in the right hand side of Eq. (A1). The polarization or ambipolar electric field intensity is then larger than that given by Eq. (A1). It was not before 1969 that this was noticed by Lemaire and Scherer (1969) and Jockers, (1970) who pointed out that the Pannekoek-Rosseland electric field is not the correct polarization electric field in the polar wind nor in the solar corona because none of these plasmas are in hydrostatic equilibrium, but rather they are accelerated away from their low altitude source regions.

A more general expression of the charge separation electric field has been derived by Ganguli et al. (1987a,b) for the case of a non-isothermal polar wind type expansion with anisotropic temperatures for the ions and electrons.

In even more general cases, the electric potential has to be determined as a solution of the Poisson's equation. But, except in thin double layer regions, the quasi-neutrality equation ($\Sigma_j Z_j n_j = 0$) is a rather satisfactory approximation, and can be used instead of Poisson's equation to obtain the polarization electric field in collisionless plasmas. The quasi-neutrality equation is usually employed to derive the electrostatic potential for which the electron density is everywhere

balanced by the total ion number density. An alternative method to employ the quasi-neutrality equation, as well as the Poisson's equation has also been proposed by Lemaire et al. (1991).

It should be pointed out that the polarization electric field intensity is generally much smaller than 0.001 mV/m. It has generally a component parallel to the magnetic field direction since the gravitational acceleration, **g,** generally has a component parallel to the magnetic field lines. Although this parallel E-field is orders of magnitudes smaller than the convection electric field, the latter is perpendicular to **u** and **B** and can always be set equal to zero by a Lorentz transformation, changing the coordinates system to a frame of reference moving with **u,** the convection velocity of the plasma; on the contrary, the parallel component of **E** is not changed in such a Lorentz transformation of coordinates.

Furthermore, note that the polarization electric field considered here is not proportional to an electric current density, **J**, as in ohmic systems. Actually, in the polar wind J = 0, but there is a non-zero polarization E-field. Of course field-aligned electric currents are not always vanishing in the magnetosphere. Field-aligned or Birkeland currents can be generated even in collisionless plasmas, like those confined in auroral flux tubes where collisions between particles can readily be ignored. This was pointed out first by Knight (1973) and Lemaire and Scherer (1974b) who derived non-linear current-potential characteristics for auroral flux tubes. In these flux tubes both cold (ionospheric) and warm (magnetospheric) electrons and ions contribute to the total electric current density and charge densities. These non-linear magnetospheric current-potential relationships were first established in the 1970's and are illustrated in Fig. A1. They are based on the exospheric expressions for the field-aligned fluxes of electrons and ions initially developed by Lemaire and Scherer (1969, 1970).

Fridman and Lemaire, (1980) showed that when the field-aligned electric potential (ΔV) ranges between 0.3 kV to 30 kV in auroral flux tubes, the Knight

current density or the more comprehensive Lemaire-Scherer current density (J) are almost linear functions of ΔV; furthermore, the energy flux of the precipitated auroral electrons is then proportional to ΔV^2. Lyons, Evans and Lundin (1979) have found experimentally that these linear and quadratic relationships are indeed verified using electron energy spectra obtained with rockets flown in the vicinity of auroral forms.

The expressions of the current-voltage characteristics for the upward current auroral region have been obtained under the assumption that, at the exobase altitude, the velocity distribution functions of the ionospheric particles and magnetospheric particles are truncated Maxwellians, just like in the theory that Jeans (1954) developed for the evaporation of neutral atoms in planetary exospheres.

The diode-like response of high-latitude plasma in magnetosphere-ionosphere coupling in the presence of field-aligned currents has also been emphasized by Mitchell et al. (1992). Other more general current-potential characteristics were derived in the 1990's by Pierrard (1997), Pierrard and Lemaire (1998), Wilson et al. (1997), and Khazanov et al. (1998) when the velocity distribution functions of particles were assumed to be generalized Lorentzian function or "kappa-functions" i.e. with an enhanced tail of suprathermal particles. The effects of non-Maxwellian velocity distribution functions on the current-potential characteristic of magnetospheric flux tubes as well as on the field-aligned distributions of exospheric plasma components, are recalled and discussed by Pierrard et al. (2006) in this issue.

Echim (2006, personal communication) currently develops new current-voltage relationships for cases where the field-aligned electric potential is not a monotonic function of the altitude as in the Pannekoek-Rosseland or Lemaire-Scherer's models, but where it has a minimum value at some altitude along auroral field lines, i.e. where the intensity of the polarization electric field reverses sign.

Appendix B: A brief overview of early polar wind measurements

In his paper, Axford (1968) made an explicit analogy between the solar wind and polar wind. The comparison of the evolution of solar wind and polar wind theories dramatically demonstrates the importance of timely and relevant observations to the development of a full understanding of a physical phenomenon. The solar wind was postulated to explain the motion of cometary tails (e.g. Biermann, 1951, 1952; Parker, 1958). The solar wind existence was verified by the earliest space experiments (see, for example, Gringauz, 1961; Bonetti et al., 1963; Snyder and Neugebauer, 1964; and Mustel, 1964). The quality of the early data facilitated direct comparison with models (e.g. Sturrock and Hartle, 1966) and there has followed a long and fruitful interchange between observers and modelers of the solar wind that has also lead to significant advances in basic plasma physics theory and observational techniques. In particular, the biggest observational impediment to understanding the polar wind was the very late realization that O^+ energization to escape velocities in the top side ionosphere was both possible and common.

Yau et al. (2006) review recent polar wind observations in this issue. Here we briefly outline the relatively few successful characterizations of the polar wind made before data from the Akebono and Polar satellites was available.

After the Axford (1968) and Banks and Holzer (1968) papers, many early investigators attempted to measure and characterize the polar wind. The most successful of them were Hoffman and his collaborators working with data from instruments on Explorer 31 (Hoffman, 1969, 1970) and ISIS-2 (Hoffman et al., 1974; Hoffman and Dodson, 1980) satellites.

The Hoffman and Dodson (1980) paper summarizes polar wind data obtained by Hoffman and his collaborators from Explorer 33 and ISIS-2 under a variety of geophysical conditions. Until the recent Akebono and Polar results, polar wind models and theories were constrained by only the data presented in the 1980

paper and a few episodic results from DE-1 as discussed below. The ISIS-2 instrument, from which almost all of the quantitative data used for comparison with polar wind theories and models was obtained, was a very sophisticated instrument for its time. It included innovative on-board data compression algorithms and a negative potential to overcome the effects of positive charging of the spacecraft (Hoffman et al., 1974).

The primary limitation of polar wind parameters derived from the ISIS data was the lack of access to high precision attitude data. The sophisticated data analysis algorithms used by Hoffman and his co-workers depended strongly on the relative angle between the spacecraft velocity and instrument look direction. In particular the ISIS-2 attitude data used by Hoffman and his colleagues was insufficiently precise to determine if the cool (~eV) O^+ population routinely detected was stationary or moving slowly (~km/s) upward or downward. Their approach to data analysis was to set the O^+ vertical drift rate equal to zero. The difficulties associated with ambiguous spacecraft potentials were mitigated by Hoffman and his colleagues in two ways. Firstly the data they used were obtained at low altitudes (<1400 km) where variations in spacecraft potential are not large (~ 1 V). Secondly the ISIS-2 instrument was biased by a negative 6 V potential which was adequate to ensure that all thermal ions were collected most of the time in the ISIS-2 orbit (Hoffman et al., 1974). Brinton et al. (1971) independently inferred the existence of the polar wind in their analysis of thermal ion mass spectrometer data obtained on Explorer 32.

More recently, the DE-1 RIMS instrument (Chappell et al., 1981) was able to episodically resolve the polar wind. Knowledge of the spacecraft attitude was not the limitation on DE-1. The limitation was that, at the higher altitudes of DE-1, variations in the spacecraft potential were significantly greater than those that could be accommodated by the maximum -8 V bias that could be applied to the RIMS instrument. Nagai et al. (1984) reported observations of the polar wind

during a geomagnetically disturbed interval where they were able to put limits on the spacecraft potential using electron measurements from the high altitude plasma instrument (Burch et al., 1981). Unfortunately only 100 days of data are available from the high altitude plasma instrument. The uncertainties in the spacecraft potential in the analyses of DE-1 RIMS data by Chappell et al. (1982) and Sojka et al. (1983) resulted in relatively larger uncertainties of polar wind parameters, particularly temperature. Chandler et al. (1991) looked at ~2000 one-minute duration distributions from DE-1 RIMS obtained at low altitudes where the combination of O^+ ram energy measurements and some ad hock assumptions made it possible to derive average densities and upward velocities for H^+, He^+, and $O^+ > 4.5$ eV. These ad hoc assumptions, however, precluded meaningful data on the H^+ temperature.

The DE-1 data from RIMS and other instruments did, however, show that significant fluxes of cool O^+ ions were escaping the ionosphere, presumably with the polar wind (e.g., Gurgiolo and Burch, 1982; Shelley et al., 1982; Lockwood et al., 1985; Chandler et al., 1991). The net result of the DE -1 observations was confusion in the theoretical and modeling community about the nature of the cool O^+ ions clearly seen with the polar wind. Were these ions an intrinsic part of the polar wind or were they added to the net outflow of ionospheric ions by processes unrelated to those forming the polar wind?

The uncertainty about the nature of O^+ in the polar wind was resolved with data that has been obtained from the SMS instrument on Akebono as discussed by Yau et al. (2006).

Acknowledgements

This work has been supported by the PRODEX-8 Grant C90179 from the *Belgian Federal Science Policy Office, Space Department*, and by *NASA* under grant NAG5-11391. Tom Chang wishes to acknowledge the generous support of *AFOSR,*

NASA, and the *NSF*. We thank the editors of this monograph, Sunny Tam, as well as Viviane Pierrard, for their collaboration and patience. We wish to also thank Dave Evans at NOAA in Boulder, Colorado, for his careful reading of an earlier version of the manuscript and for his valuable comments. Lastly, we would like to express our warm appreciation to Vanessa George, LASP, University of Colorado, for her time spent editing the text and references of this paper.

References

Abe, T., Whalen, B.A., Yau, A.W., Horita, R.E., Watanabe, S., Sagawa, E., 1993. EXOS D (Akebono) suprathermal mass spectrometer observations of the polar wind, J. of Geophys. Res. 98, 11191.

Abe, T., Yau, A.W., Watanabe, S., Yamada, M., Sagawa, E., 2003. Long-term variation of the polar wind velocity and its implication for the ion acceleration process: Akebono/suprathermal ion mass spectrometer observations, J. of Geophys. Res. 109, A09305, doi:10.1029/2003JA010223.

Aldrich, T.L., Neir, A.O., 1948. The occurrence of ^{3}He in natural sources of helium, Phys. Rev. 74, 1590.

Alvarez, L.W., Cornog, R., 1939. Helium and hydrogen of mass 3, Phys. Rev. 56, 613.

Axford, W.I., 1968. The polar wind and the terrestrial helium budget, J. of Geophys. Res. 73, 6855-6859.

Axford, W.I., Hines, C.O., 1961. A unifying theory of high-latitude geophysical phenomena and geomagnetic storms, Can. J. Phys. 39, 1433.

Banks, P.M., Holzer, T.E., 1968. The polar wind, J. of Geophys. Res. 73, 6846-6854.

Banks, P.M., Holzer, T.E., 1969a. Reply, J. of Geophys. Res. 74, 3734-3739.

Banks, P.M., Holzer, T.E., 1969b. High-latitude plasma transport: The polar wind, J. of Geophys. Res. 74, 6317.

Banks, P.M., Kockarts, G., 1973. *Aeronomy*, Academic Press, New York,

Banks, P.M., Nagy, A.F., Axford, W.I., 1971. Dynamical behavior of thermal protons in the mid-latitude ionosphere, and magnetosphere, Planet. Space Sci. 19, 1053.

Barakat A.R., Schunk, R.W., 1982a. Transport equations for multi-component anisotropic space plasmas: a review, Plasma Physics 24, 389.

Barakat, A.R., Schunk, R.W., 1982b. Comparison of transport equations based on Maxwellian and bi-Maxwellian distributions for anisotropic plasmas, J. Phys. D: Appl. Phys. 15, 1195.

Barakat, A.R., Schunk, R.W., 1982c. Comparison of Maxwellian and bi-Maxwellian expansions with Monte-Carlo simulations for anisotropic plasmas, J. Phys. D: Appl. Phys. 15, 2189.

Barakat, A.R., Schunk, R.W., 1983. O^+ Ions in the Polar Wind, J. of Geophys. Res. 88, 7887.

Barakat, A.R., Schunk, R.W., 1984. Effect of the hot electrons on the polar wind, J. of Geophys. Res. 89, 9771.

Barakat, A.R., Schunk, R.W., 2001. Effects of wave-particle interactions on the dynamic behavior of the generalized polar wind, J. Atmos. Sol. Terr. Phys. 63, 75-83.

Barakat, A.R., Barghouthi I.A., Schunk, R.W., 1995. Double-hump H^+ velocity distribution in the polar wind, Geophys. Res. Lett. 22, 1857-1860.

Barakat, A.R., Demars, H.G., Schunk, R.W., 1998a. Dynamic features of the polar wind in the presence of hot magnetospheric electrons, J. of Geophys. Res. 103, 29289-29303.

Barakat, A.R., Thiemann, H., Schunk, R.W., 1998b. Comparison of macroscopic PIC and semi-kinetic models of the polar wind, J. of Geophys. Res. 103, 29277-

29287.

Barakat, A.R., Schunk, R.W., Barghouthi, I.A., Lemaire, J., 1990. Monte Carlo study of the transition from collision-dominated to collisionless polar wind flow, in *Physics of Space Plasmas* (1990), SPI Conference Proceedings and Reprints Series, No. 10, edited by T. Chang, J. Crew, and J.R. Jasperse, pp. 431-437, Scientific Publishers, Cambridge, Massachusetts.

Barakat, A.R., Schunk, R.W., Demars, H.G., 2003. Seasonal and solar activity dependence of the generalized polar wind with low-altitude auroral ion energization, J. of Geophys. Res. 108, A11, 1405, doi:10.1029/2002JA009360.

Barghouthi, I.A., Barakat, A.R., Schunk, R.W., 1993. Monte Carlo study of the transition region in the polar wind: an improved collision model, J. of Geophys. Res. 98, 17583.

Bates, D.R., McDowell, M.R.C., 1957. Atmospheric helium, J. Atmos Sol. Terr. Phys. 11, 200.

Bates, D.R., McDowell, M.R.C., 1959. Escape of helium, J. Atmos. Sol. Terr. Phys. 16, 393.

Bates, D.R., Patterson, T.N.L., 1962. Helium ions in the upper atmosphere, Planetary and Space Science 9, 599.

Bauer, S.J., 1966. The constitution of the topside ionosphere, in Electron Density Profiles in Ionosphere and Exosphere, Jon Frihagen, ed., North Holland, Amsterdam, p. 271.

Biermann, L., 1951. Kometenschweife und solare Korpuskularstrahlung, Zeitschrift fur Astrophysik 29, 274.

Biermann, L., 1952. Uber de Schweif des Kometen Halley im Jare 1910, Zeitschrift für Naturforshung 7a, 127.

Bonetti, A., Bridge, H., Lazarus, A., Rossi, B., Scherb, F., 1963. Explorer 10 plasma measurements, J. of Geophys. Res. 68, 4017.

Brinton H.C., Grebowsky, J.M., Mayr, H.G., 1971. Altitude variation of ion composition in the midaltitude trough region: Evidence for upward plasma flow, J. of Geophys. Res. 76, 3738.

Burch, J.L., Winningham, J.D., Blevins, V.A., Eaker, N., Gibson, W.C., Hoffman, R.A., 1981. The high-altitude plasma instrument for Dynamics Explorer -A, Space Sci. Instrumentation 5, 455.

Carpenter, D.L., 1963. Whistler evidence of a 'knee' in the magnetospheric ionization density profile, J. of Geophys. Res. 68, 1675.

Chamberlain, J.W., 1960. Interplanetary gas, 2, Expansion of a model solar corona, Astrophys. J. 131, 47-56.

Chandler, M.O., Waite, J.H., Jr., Moore, T.E., 1991. Observations of polar ion outflows, J. of Geophys. Res. 96, 1421.

Chandrasekhar, S., 1960. Hydrodynamic and hydromagnetic stability, *Plasma Physics*, International Series of Monographs on Physics, University of Chicago, Clarendon.

Chappell, C.R., Fields, S.A., Baugher, C.R., Hoffman, J.H., Hanson, W.B., Wright, W.W., Hammack, H.D., Carignan, G.R., Nagy, A.F., 1981. The retarding ion mass spectrometer on Dynamcs Explorer -A, Space. Sci. Instrumentation 5, 477.

Chappell, C.R., Green, J.L., Johnson, J.F.E., Waite, J.H., Jr., 1982. Pitch angle variations in magnetospheric thermal plasma – Initial observations from Dynamics Explorer 1, Geophys. Res. Lett. 9, 933.

Chew, G.F., Goldberg, M.L., Low, F.E., 1956. The Boltzmann equation and the one-fluid hydromagnetic equations in the absence of particle collisions, Proc. R. Soc., London A, 236, 112.

Chiu, Y.T., Schulz, M., 1978. Self-consistent particle and parallel electrostatic field distributions in the magnetospheric-ionospheric auroral region, J. of Geophys. Res. 83, 629-642.

Chodura, R., Pohl, F., 1971. Hydrodynamic equations for anisotropic plasmas in magnetic fields. II. Transport equations including collisions, Plasma Physics 13, 8, 645-658.

Collier, M.R., 1993. On generating kappa-like distribution functions using velocity space Levy flights, Geophys. Res. Lett. 20, 1531.

Collier, M.R., Hamilton, D.C., 1995. The relationship between kappa and temperature in energetic ion spectra at Jupiter, Geophys. Res. Lett. 22, 303.

Demars, H.G., Schunk, R.W., 1979. Transport equations for multispecies plasmas based on individual bi-Maxwellian distributions, J. Phys. D. Appl. Phys. 12, 1051.

Demars, H.G., Schunk, R.W., 1991. Comparison of semikinetic and generalized transport models of the polar wind, Geophys. Res. Lett. 18, 713-716.

Demars, H.G., Schunk, R.W., 1992. Semikinetic and generalized transport models of the polar and solar winds, J. of Geophys. Res. 97, 1581-1595.

Demars, H.G., Barakat, A.R., Schunk, R.W., Thiemann, H., 1996a. Shocks in the polar wind, Geophys. Res. Lett. 23, 1721-1724.

Demars, H.G., Barakat, A.R., Schunk, R.W., 1996b. Effect of centrifugal acceleration on the polar wind, J. of Geophys. Res. 101, 24,565-24,571.

Demars, H.G., Barakat, A.R., Schunk, R.W., 1998. Trapped particles in the polar wind, J. of Geophys. Res. 103, 419.

Demars, H.G., Schunk, R.W., Barakat, A.R., 1999. Comparing fluid and particle-in-cell solutions for the polar wind, J. of Geophys. Res. 104, 28,535-28,545.

Dessler, A.J., Cloutier, P.A., 1969. Discussion of letter by Peter M. Banks and

Thomas E. Holzer, in *The Polar Wind,* J. of Geophys. Res. 74, 3730-3733.

Dessler, A.J., Michel, F.C., 1966. Plasma in the geomagnetic tail, J. of Geophys. Res. 71, 1421.

Dessler, A.J., Cloutier, P.A., Hanson, W.B., Midgley, J.E., 1968. The polar breeze (abstract), Trans. AGU 49, 749.

Donahue, T.M., 1971. Polar ion flow: wind or breeze? Rev. Geophys. Sp. Phys. 9, 1-9.

Dungey, J.W., 1961. Interplanetary magnetic field and the auroral zones, Phys. Rev. Lett. 6, 47.

Ergun, R.E., and 12 others, 2000. Feasibility of a multisatellite investigation of the Earth's magnetosphere with radio tomography, J. of Geophys. Res. 105, 361-374.

Eviatar, A., Lenchek, A.M., Singer, S.F., 1964. Distribution of density in an ion-exosphere of a non-rotating planet, Phys. Fluids 7, 1775.

Fahr, H.J., Shizgal, B., 1983. Modern exospheric theories and their observational relevance, Rev. of Geophysics and Space Phys. 21, 75-124.

Fridman, M., Lemaire, J., 1980. Relationship between auroral electrons fluxes and field-aligned electric potential difference, J. of Geophys. Res. 85, 664-70.

Fung, S.F., Hoffman, R.A., 1991. A search for parallel electric fields by observing secondary electrons and photoelectrons in the low-altitude auroral zone, J. of Geophys. Res. 96, 3533.

Ganguli, S.B., 1996. The polar wind, Reviews of Geophys. 34, 311.

Ganguli, S.B., Palmadesso, P.J., 1987a. Plasma transport in the auroral return current region, J. of Geophys. Res. 92, 8673-8690.

Ganguli, S.B., Mitchell, H.G., Jr., Palmadesso, P.J., 1987b. Behavior of the ionized plasma in the topside ionosphere: the polar wind, Planet. Space Sci. 35, 703.

Gombosi, T.I., Nagy, A.F., 1989. Time-dependent modeling of field-aligned current-generated ion transients in the polar wind, J. of Geophys. Res. 94, 359.

Gombosi, T.I., Cravens, T.E., Nagy, A.F., 1985. A time dependent theoretical model of the polar wind: Preliminary results, Geophys. Res. Lett. 12, 167.

Grad, H., 1949. On kinetic theory of rarefied gases, Comm. Pure Appl. Math. 2, 331.

Grad, H., 1958. Principles of the kinetic theory of gases, in Handbuch der Physik, vol. 12, p. 205, Springer-Verlag, Berlin.

Gringauz, K.I., 1961. Some results of experiments in interplanetary space by means of charged particle traps on Soviet space probes, Space Research, 2, 539.

Gurgiolo, C., Burch, J.L., 1982. DE-1 observation of the polar wind – A heated and an unheated component, Geophys. Res. Lett. 9, 945-948.

Hartle, R.E., 1969. Ion-Exosphere with Variable Conditions at the Baropause, Physics of Fluids 12, 455-462.

Hartle, R.E., 1971. Model for Rotating and Nonuniform Planetary Exospheres, Physics of Fluids 14, 2592-2598.

Hinton, F.L., 1983. Collisional Transport in Plasma, in *Basic Plasma Physics I and II,* edited by A.A. Galeev and R.N. Sudan, p. 149-200, North-Holland Publishing Company, Amsterdam.

Ho, C.W., Horwitz, J.L., Wilson, G.R., 1991. Effects of a sudden impulse in electron temperature on the polar wind: A time-dependent semi-kinetic models, in *Modelling Magnetospheric Plasma Processes*, AGU Geophys. Monograph Series, Vol. 62, edited by G.R. Wilson, and M. Chandler, p. 105, Washington, DC.

Ho, C.W., Horwitz, J.L., Wilson, G.R., Singh, N., Moore, T.E., 1992. Effects of magnetospheric electrons on polar plasma outflow a semi-kinetic model, J. of Geophys. Res. 97, 8425.

Hoffman, J.H., 1969. Ion mass spectrometer on Explorer 31 satellite, Proc. IEEE, 57, 1063-1067.

Hoffman, J.H. 1970. Studies of the composition of the ionosphere with a magnetic deflection mass spectrometer, Int. J. Mass. Spectrom. Ion. Phys. 4, 315.

Hoffman, J.H., Dodson, W.H., 1980. Light ion concentrations and fluxes in the polar regions during magnetically quiet times, J. of Geophys. Res. 85, 626.

Hoffman, J.H., Dodson, W.H., Lippincott, C.R., Hammack, H.D., 1974. Initial ion composition results from the ISIS 2 satellite, J. of Geophys. Res. 79, 4246.

Holzer, T.E., Fedder, J.A., Banks, P.M., 1971. A comparison of kinetic and hydrodynamic models of an expanding ion-exosphere, J. of Geophys. Res. 76, 2453-2468.

Horita, R.E., Yau, A.W., Whalen, B.A., Abe, T., Watanabe, S., 1993. Ion depletion zones in the polar wind - EXOS D suprathermal ion mass spectrometer observations in the polar cap, J. of Geophys. Res. 98, 11,439-11,448.

Horwitz, J.L., Ho, C.W., Scarbro, H.D., Wilson, G.R., Moore, T.E., 1994. Centrifugal acceleration of the polar wind, J. of Geophys. Res. 99, 15051.

Huang, T.S., Birmingham, T.J., 1992. The polarization electric field and its effects in an anisotropic rotating magnetospheric plasma, J. of Geophys. Res. 97, 1511.

Jeans, J.H., 1954. The Dynamical Theory of Gases, 4th Ed., p. 245, Dover, New York.

Jockers, K., 1970. Solar wind models based on exospheric theory, Astron. Astrophysics 6, 219-239.

Kamiyama, H., Takaki, H., 1966. A possible distribution of ion density in the iono-exosphere with a dipole magnetic field, J. Geomagn. Geoelectr. 18, 1-11.

Khazanov, G.V., Liemohn, M.W., Moore, T.E., 1997a. Photoelectron effects on the self-consistent potential in the collisionless polar wind, J. of Geophys. Res. 102,

7509.

Khazanov, G.V., Liemohn, M.W., Moore, T.E., 1997b. Combined effects of photoelectrons, the ponderomotive force, and precipitation in the dynamics of high-latitude ion outflows, Eos Trans. AGU, 78(17), 1997 Spring Meet. Suppl., S290.

Khazanov, G.V., Liemohn, M.W., Krivorutsky, E.N., Moore, T.E., 1998. Generalized kinetic description of a plasma in an arbitrary field-aligned potential energy structure, J. of Geophys. Res. 6871-6889.

Knight, S., 1973. Parallel electric fields, Planet. Space Sci. 21, 741.

Kockarts G., 1973. Helium in the terrestrial atmosphere, Space Science Rev. 14, 723-757.

Kockarts, G., Nicolet, M., 1962. Le problème aéronomique de l'hélium et de l'hydrogène neutres. Annales de Géophysique 18, 269.

Lemaire, J., 1972a. O^+, H^+ and He^+ ion distributions in a new polar wind model, J. Atmos. Sol. Terr. Phys. 34, 1647-1658.

Lemaire, J., 1972b. Effect of escaping photoelectrons in a polar exospheric model, Space Research 12, 1413.

Lemaire, J.F., Gringauz, K.I., with contributions from D.L. Carpenter and V. Bassolo, 1968. The Earth's Plasmasphere, Cambridge University Press, New York, p. 350.

Lemaire, J., Scherer, M., 1969. Le champ électrique de polarisation dans l'exosphère ionique polaire, Compt. Rend. l'Acad. Sci., Paris, 269B, 666-669.

Lemaire, J., Scherer, M., 1970. Model of the polar ion-exosphere, Planet. Space Sci. 18, 103.

Lemaire, J., Scherer, M., 1971. Simple model for an ion-exosphere in an open magnetic field, Phys. Fluids 14, 1683.

Lemaire, J., Scherer, M., 1972. Ion-exosphere with asymmetric velocity distribution, Phys. Fluids 15, 760-766.

Lemaire, J., Scherer, M., 1973. Kinetic models of the solar and polar winds, Rev. Geophys. Sp. Phys. 11, 427-468.

Lemaire, J., Scherer, M., 1974a. Exospheric models of the topside ionosphere, Sp. Sci. Rev. 11, 591-640.

Lemaire, J., Scherer, M., 1974b. Ionosphere-plasmasheet field-aligned current and parallel electric fields, Planet. Space Sci. 22, 21485.

Lemaire, J., Scherer, M., 1978. Field-aligned distribution of plasma mantle and ionospheric plasmas, J. Atmos. Sol. Terr. Phys. 40, 337-342.

Lemaire, J., Barakat, A., Lesceux, J.M., Shizgal, B., 1991. A method for solving Poisson's equation in geophysical and astrophysical plasmas, in *Rarefied Gas Dynamics*, Ed. A.E. Beylich, VCH Verlagsgesellschaft MbH, p. 417-424.

Lie-Svendsen, O., Rees, M.H., 1996. An improved kinetic model for the polar outflow of a minor ion, J. of Geophys. Res. 101, 2415.

Lockwood, M., Chandler, M.O., Horwitz, J.L., Waite, J.H., Jr., Moore, T.E., Chappell, C.R., 1985. The cleft ion fountain, J. of Geophys. Res. 90, 9736.

Longmire, C.L., 1963. *Elementary Plasma Physics*, Interscience Publishers, John Wiley and Sons, New York, p. 296.

Lyons, L.R., Evans, D.S., Lundin, R., 1979. An observed relation between magnetic field-aligned electric fields and downward electron energy fluxes in the vicinity of auroral forms, J. of Geophys. Res. 84, 457.

MacDonald, G.J.F., 1963. The escape of helium from the Earth's atmosphere, Reviews of Geophysics 1, 305.

Mange, P., 1960. The distribution of minor ions in electrostatic equilibrium in the

high atmosphere, J. of Geophys. Res. 65, 3833-3834.

Mange, P., 1972. The exosphere and geocorona, in Solar-Terrestrial Physics/1970, Part. 4, The Upper Atmosphere, edited by E.R. Dyer, p. 68-86, D. Reidel, Dordrecht, Netherlands.

Marubashi, K., 1970. Escape of the polar-ionospheric plasma into the magnetospheric tail, Rep. Ionos. Sp. Res., Japan, 24, 322-346.

Mitchell, H.G., Jr., Palmadesso, P.J., 1983. A dynamic model for the auroral field line plasma in the presence of field-aligned current, J. of Geophys. Res. 88, 2131.

Mitchell, H.G., Jr., Ganguli, S.B., Palmadesso, P.J., 1992. Diode-like response of high-latitude plasma in magnetosphere-ionosphere coupling in the presence of field-aligned currents, J. of Geophys. Res. 97, 12 045.

Mustel, E.R., 1964. The sun and interplanetary plasma, Space Research 4, 77.

Nagai, T., Waite, J.H., Jr., Green, J.L., Chappell, C.R., 1984. First measurements of supersonic polar wind in the polar magnetosphere, Geophys. Res. Lett. 11, 669.

Ness, N.F., 1965. The Earth's magnetic tail, J. of Geophys. Res. 70, 2989-3005.

Nicolet, M., 1957. The aeronomic problem of helium, Ann. Geophys. 13, 1.

Nicolet, M., 1961. Helium, an important constituent in the lower exosphere, J. of Geophys. Res. 66, 2263-2264.

Nishida, A., 1966. Formation of plasmapause, or magnetospheric plasma knee, by the combined action of magnetospheric convection and plasma escape from the tail, J. of Geophys. Res. 71, 5669-5679.

Öpik, E.J., Singer, S.F., 1959. Distribution of density in a planetary exosphere, Phys. Fluids 2, 653-655.

Öpik, E.J., Singer, S.F., 1960. Distribution of density in a planetary exosphere, I., Phys. Fluids 3, 486-488.

Öpik, E.J., Singer, S.F., 1961. Distribution of density in a planetary exosphere, II, Phys. Fluids 4, 221-233.

Oraevskii, V., Chodura, R., Feneberg, W., 1968. Hydrodynamic equations for plasmas in strong magnetic fields, I. Collisionless approximation, Plasma Phys. 10, 819.

Pannekoek, A., 1922. Ionization in stellar atmospheres, Bull. Astron. Inst. Netherlands, 1, 107-118.

Parker, E.N., 1958. Dynamics of the interplanetary gas and magnetic field, Astrophys. Journal 128, 664-676.

Parker, E.N., 1963. Interplanetary dynamical processes, Interscience Publishers, John Wiley and Sons, New York, p. 272.

Parks, G.K., 2004. *Physics of Space Plasmas, An Introduction,* Second Edition, Advanced Book Program, Westview Press, Boulder, Colorado.

Peterson, W.K., Doering, J.P., Potemra, T.A., Bostrom, C.O., Brace, L.H., Heelis, R.A., Hanson W.B., 1977. Measurement of magnetic field-aligned potential differences using high resolution conjugate photoelectron energy spectra, Geophys. Res. Lett. 4, 373.

Pierrard, V., Fonctions de distribution des vitesses des particules s'échappant de l'ionosphère, PhD Thesis, UCL, 1997.

Pierrard, V., Lemaire, J., 1996. Lorentzian ion exosphere model, J. of Geophys. Res. 101, 7923.

Pierrard, V., Lemaire, J., 1998. A collisional kinetic model of the polar wind, J. of Geophys. Res. 103, 11701-11709.

Pierrard, V., Khazanov, G.V., Lemaire, J., 2006. Current-voltage relationship, accepted for publication in J. Atmos. Sol. Terr. Phys., Special issue on the polar wind, this volume.

Rosseland, S., 1924. Electrical state of a star, Monthly Notices Royal Astronomical Soc. 84, 720-728.

Schunk, R.W., 1975. Transport equations in aeronomy, Planet. Space Sci. 23, 437.
Schunk, R.W., 1977. Mathematical structure of transport equations for multispecies flows, Rev. Geophys. Sp. Phys. 15, 429.

Schunk, R.W., 1986. An updated theory of the polar wind, Advance Space Research 6 (3), 79.

Schunk, R.W., 1988. Polar wind tutorial, in *Physics of Space Plasmas*, SPI Conf. proc. Reprint Ser., edited by T. Chang, G.B. Crew, and Jaspere, p. 81, Scientif, Cambridge, Massachusetts.

Schunk, R.W., Sojka, J.J., 1989. A three-dimensional time-dependent model of the polar wind, J. of Geophys. Res. 94, 8973-8991.

Schunk, R.W., Sojka, J.J., 1997. Global ionosphere-polar wind system during changing magnetic activity, J. of Geophys. Res. 102, 11625-11651.

Schunk, R.W., Watkins, D.S., 1981. Electron temperature anisotropy in the polar wind, J. of Geophys. Res. 86, 91.

Schunk, R.W., Watkins, D.S., 1982. Proton temperature anisotropy in the polar wind, J. of Geophys. Res. 87, 171.

Shelley, E.G., Peterson, W.K., Ghielmetti, A.G., Geiss, J., 1982. The polar ionosphere as a source of energetic magnetospheric plasma, Geophys. Res. Lett. 9, 941.

Shizgal, B., Arkos, G.G., 1996. Nonthermal escape of the atmospheres of Venus, Earth and Mars, Reviews of Geophysics 34, 483-505.

Shizgal B., Blackmore, R., 1984. A discrete ordinate method of solution of linear boundary value and eigenvalue problems, J. Comput. Phys. 55, 313-327.

Singer, S.F., 1960. Structure of the Earth's Exosphere, Journal of Geophy. Res. 65,

2577.

Singh, N., Schunk, R.W., 1985. Temporal behavior of density perturbations in the polar wind, J. of Geophys. Res. 90, 6487.

Snyder, C.W., Neugebauer, M., 1964. Interplanetary solar-wind measurements by Mariner II, Space Research 4, 89-113.

Sojka, J.J., Schunk, R.W., Johnson, J.F.E., Waite, J.H., Chappell, C.R., 1983. Characteristics of thermal and suprathermal ions associated with the dayside plasma trough as measured by the Dynamics Explorer Retarding Ion Mass Spectrometer, J. of Geophys. Res. 88, 7895.

Spitzer, L., Jr., 1949. The terrestrial atmosphere above 300 km, in G.P. Kuiper (ed.), The atmospheres of the Earth and Planets, Univ. Chicago Press, Illinois, p. 213-249.

Spitzer, L., Jr., 1956. *Physics of Fully Ionized Gases,* p. 105, Wiley-Interscience, New York.

Sturrock, P.A., Hartle, R.E., 1966. Two-fluid model of the solar wind, Physical Review Letters 16, 14, 628-631.

Summers, D., Thorne, R.M., 1992. A new tool for analyzing microinstabilities in space plasmas modeled by a generalized Lorentzian (Kappa) distribution, J. of Geophys. Res. 97, 16827.

Tam, S.W.Y., Yasseen, F., Chang, T., Ganguli, S.B., 1995a. Self-consistent kinetic photoelectron effects on the polar wind, Geophys. Res. Lett. 22, 2107.

Tam, S.W.Y., Yasseen, F., Chang, T., Ganguli, S.B., Retterer, J.M., 1995b. Anisotropic kinetic effects of photoelectrons on polar wind transport, in Cross-Scale Coupling in Space Plasmas, edited by J.L. Horwitz, N. Singh, and J.L. Burch, AGU Geophys. Monograph Series, Vol. 93, p. 133, Washington, D.C.

Tam, S.W.Y., Yasseen, F., Chang, T., 1998. Further development in theory/data closure of the photoelectron-driven polar wind and day-night transition of the outflow, Ann. Geophys. 16, 948.

Tam, S.W.Y., Chang, T., Pierrard, V., 2006. Kinetic modeling of the polar wind, accepted for publication in J. Atmos. Sol. Terr. Phys., Special issue on the polar wind, this volume.

Taylor, H.A., Jr., 1972. The light ion trough. Planetary and Space Science 20, 1593-1605.

Taylor, H.A, Jr., Brinton, H.C., Carpenter, D.L., Bonner, F.M., Heyborne, R.L., 1969. Ion depletion in the high-latitude exosphere. Simultaneous OGO 2 observations of the light ion trough and the VLF cutoff, J. of Geophys. Res. 74, 3517-3528.

Treumann, R.A., 1997. Theory of super-diffusion for the magnetopause, Geophys. Res. Lett. 24, 1727-1730.

Vasyliunas, V.M., 2001. Electric field and plasma flow: What drives what? Geophys. Res. Lett. 28, 2177-2180.

Wilson, A.T., 1962. A proposed electrostatic acceleration mechanism in the upper atmosphere and its bearing on the helium problem, J. of Geophys. Res. 67, 4501.

Wilson, G.R., Ho, C.W., Horwitz, J.L., Singh, N., Moore, T.E., 1990. A new kinetic model for time-dependent polar plasma outflow: initial results, Geophys. Res. Lett. 17, 263.

Wilson, G.R., Khazanov, G.V., Horwitz, J.L., 1997. Achieving zero current for polar wind outflow on open flux tubes subjected to large photoelectron fluxes, Geophys. Res. Lett. 24, 1183.

Winningham, J.D., Gurgiolo, C., 1982. DE-2 photoelectron measurements consistent with a large scale parallel electric field over the polar cap, Geophys. Res. Lett. 9, 977.

Yasseen, F., Retterer, J.M., 1991. Critical points in the 16-moment approximation, J. of Geophys. Res. 96, 1827.

Yasseen, F., Retterer, T., Chang, T.S., Winningham, J.D., 1989. Monte-Carlo modeling of polar wind photoelectron distributions with anomalous heat flux, Geophys. Res. Lett. 16, 1023.

Yau, A.W., Abe, T., Peterson, W.K., 2006. The Polar Wind: Recent Observation, accepted for publication in J. Atmos. Sol. Terr. Phys., Special issue on the polar wind, this volume.

Yau, A.W., Whalen, B.A., Abe, T., Mukai, T., Oyama, K.I., Chang, T., 1995. Akebono observations of electron temperature anisotropy in the polar wind, J. of Geophys. Res. 100, 17451.

Zinin, L.V., Galperin, Y.I., Latyshev, K.S., Grigoriev, S.A., 1985. Non-stationary field-aligned fluxes of thermal ions O^+ and H^+ outside the plasmapause; Refinement of the polar wind theory, in *Results of the Arcad 3 Project and of the recent Programmess in the Magnetospheric and Ionospheric Physics*, Trans. of International Symposium Toulouse, 1984, p. 391, Cepadues, Toulouse, France.

Figures

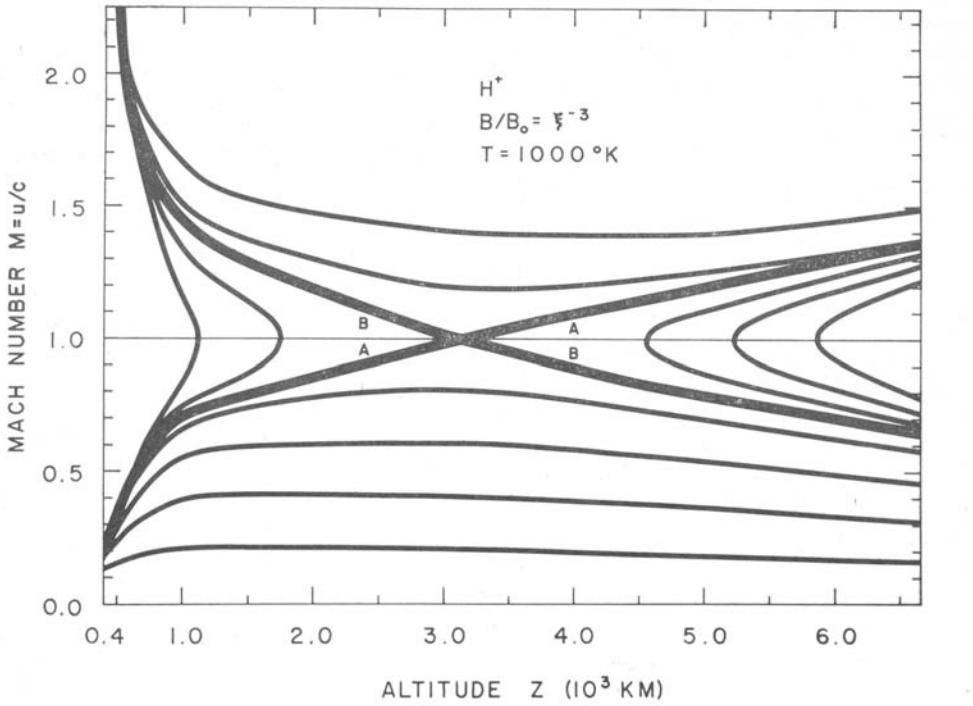

Fig 1. Solutions for the H^+plasma Mach number as a function of altitude when the plasma is isothermal, when ion friction as well as ion production and loss are included. The ascending critical solution, shown by the heavy line marked A, is the only only solution which gives a low speed at low altitudes coupled with zero charged particle pressure at infinity. The point of transition to supersonic flow occurs where M= 1. Subsonic solutions occur when the imposed plasma pressure boundary condition is greater than the asymptotic pressure of the descending critical solution (curve B) (from Banks and Holzer, 1968).

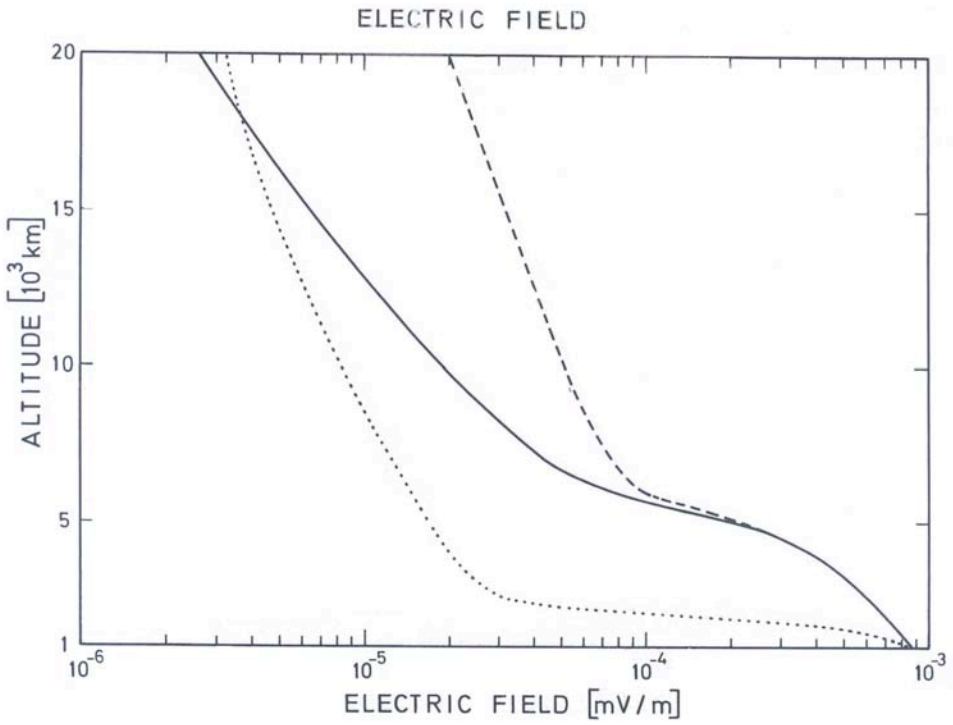

Fig. 2. Parallel electric field distribution along an open geomagnetic field line intersecting the exobase at a dip-latitude of 85° in three categories of exospheric polar wind models. The exobase is located at 960 km altitude. The exobase temperatures of the O^+, H^+, He^+ ions and electrons are respectively 1500 K, 4000 K, 3750 K, and 4500 K. The solid line corresponds to the model in which the trapped and incoming particles are missing. The dashed line corresponds to the "trapped" exospheric model where only incoming particles are missing, and the dotted line corresponds to the barometric model where all classes of trajectories are equally populated by particles in isothermal equilibrium. The latter model corresponds to the hydrostatic model where all particles are in diffusive equilibrium. Note that the electric field intensity in this barometric model is the Pannekoek-Rosseland electric field. It is smaller than in the two other exospheric models for which some classes of trajectories are missing and for which net polar wind flows of H^+ and He^+ ions are escaping out of the topside ionosphere (Lemaire and Scherer, 1974a).

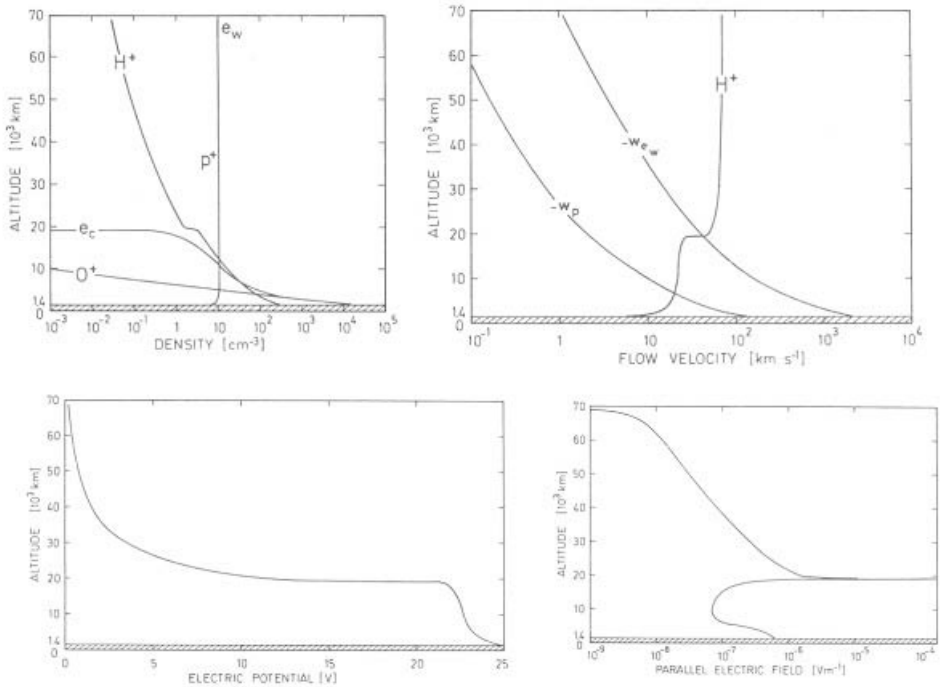

Fig 3. Polar cusp flux tube filled with escaping cold ionospheric plasma (0^+, H^+, e_c) and warm magnetosheath plasma (p^+, e_w); field-aligned distributions of ion and electron densities (upper left panel), bulk velocity (upper right panel), electric potential (lower left panel), and electric field (lower right panel) (from Lemaire and Scherer, 1978).

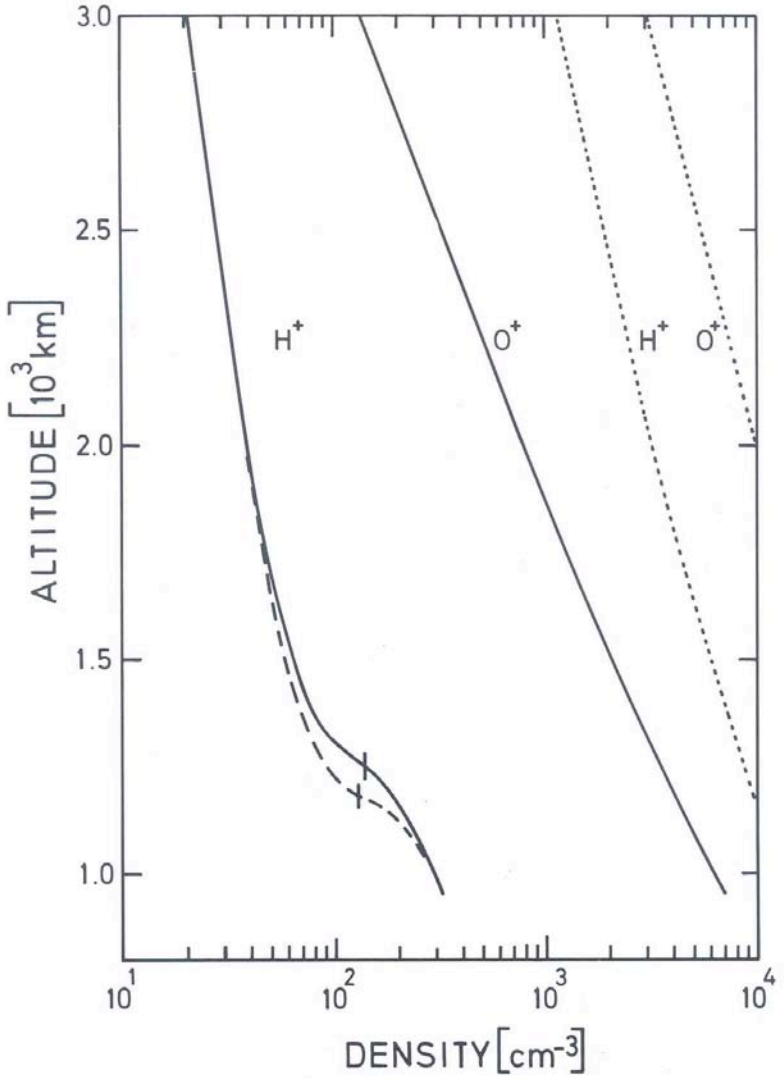

Fig 4. Oxygen and hydrogen ion densities versus altitude in exospheric and hydrodynamic polar wind models. The solid lines correspond to a symmetric ($u_H+ = 0$) truncated Maxwellian exospheric model fitted to a hydrodynamic model (hybrid kinetic-hydrodynamic model); the matching of both solutions has been made across the exobase level indicated by a vertical bar. The dashed line corresponds to an asymmetric exospheric model for which the VDF is a displaced (asymmetric) Maxwellian with $u_H+ = 1.4$ km/s. The dotted lines show the O^+ and H^+ density distributions in the full hydrodynamic model of Banks and Holzer (1969a). In all these models it is assumed that the electron and ion temperatures are equal to 3000 K. (from Lemaire, 1972a).

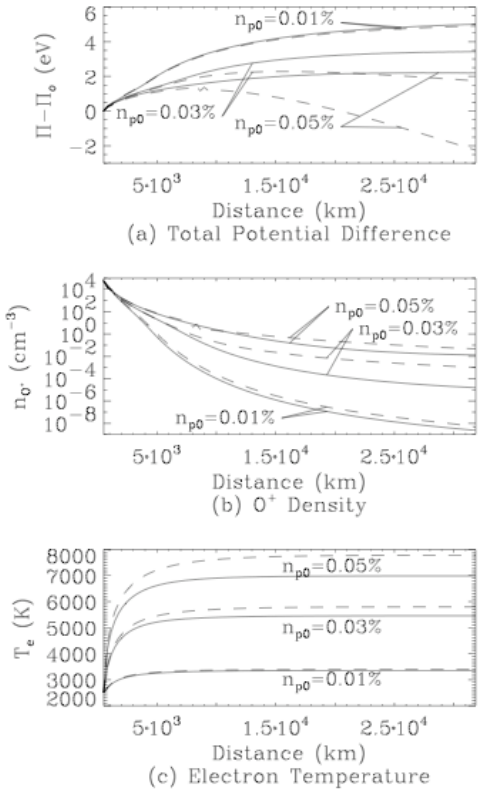

Fig 5. Comparison of the results from Khazanov et al. (1997a) (solid lines) with those of the third generation exospheric polar wind model in the isotropic Maxwellian case (dashed lines). Three values of n_{p0}, the photoelectron content at the base of the run (500 km), are shown along the field line for (a) total potential difference (electrostatic and gravitational) for O^+, (b) O^+ density, and (c) thermal electron temperature (Khazanov et al., 1998).

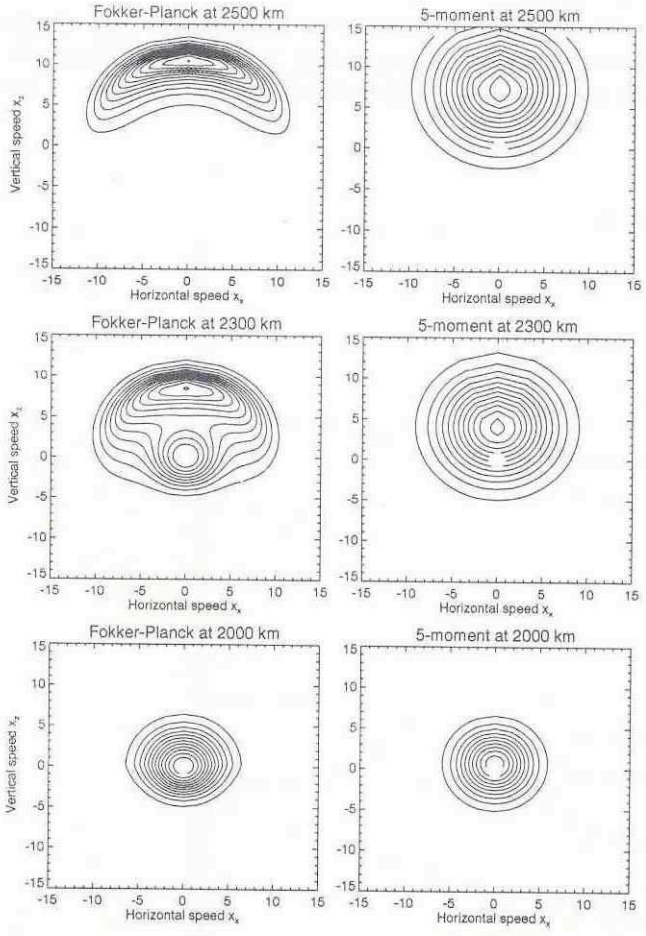

Fig 6. Velocity distribution functions of polar wind H^+ ions at three different altitudes in the polar wind. The isocontours are meridional cross-sections of the VDF. In the left-hand side panels they are determined by Lie-Svendsen and Rees (1996) Fokker-Planck equation using a standard finite difference method. The solutions shown in the right hand side panels are those inferred from the solutions of the 5-moments equations and Grad's kinetic theory of non-uniform gases. The H^+ ions are accelerated through a background of O^+ ions and neutralizing thermal electrons by the internal electric field produced inside the plasma by gravitational charge separation. Note the development of a secondary maximum in VDF in the Fokker-Planck solution. Note that in the right hand side the VDF has a single maximum at a velocity equal to the mean velocity of the particles, which corresponds to the bulk speed of the polar wind H^+ ions (from Lie-Svendsen and Rees, 1996).

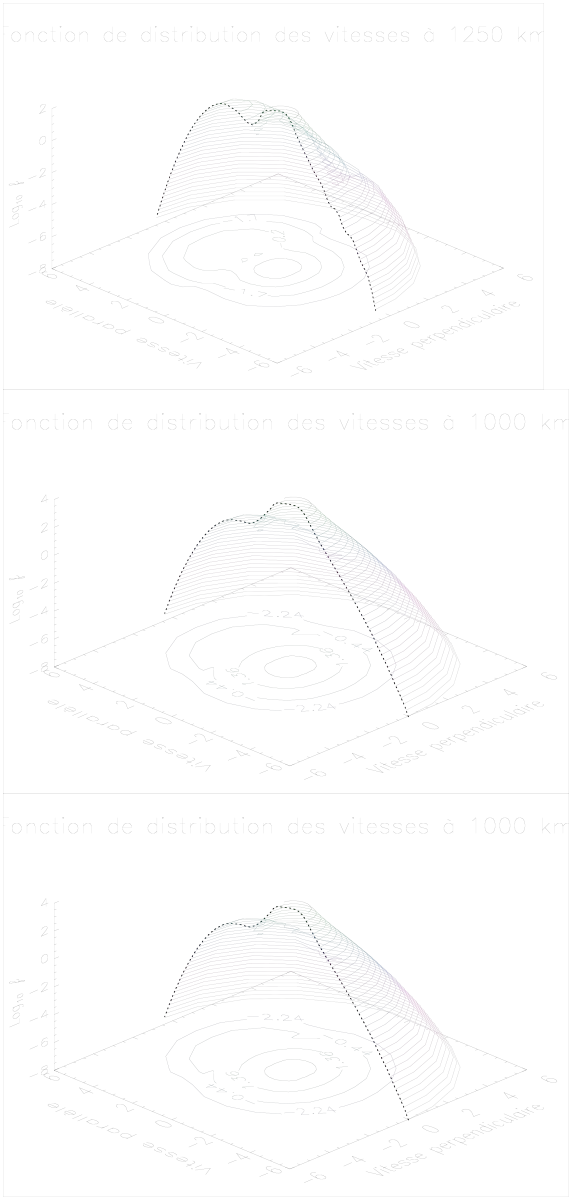

Fig 7. 2D and 3D representations of the H^+ velocity distribution function obtained as a solution of the Fokker-Planck equation at three different altitudes in the transition region. The velocities parallel and perpendicular to the magnetic field lines are normalized to the thermal ion velocity of the hydrogen ions. The polar wind H^+ ions are accelerated upward by the Pannekoek-Rosseland electric field produced by gravitational charge separation in the background plasma dominated by the O^+ ions. Note the formation of a secondary peak in the suprathermal tail of the VDF. It is this emerging peak that carries most of the upward flux of particles and energy; it becomes more and more prominent when the altitude increases. The primary peak centered on $\mathbf{v} = 0$ corresponds to the population of H^+ ions that have a small velocity and a large Coulomb collision cross-section; this is why the VDF around this peak is nearly a Maxwellian and isotropic one (from Pierrard, 1997).

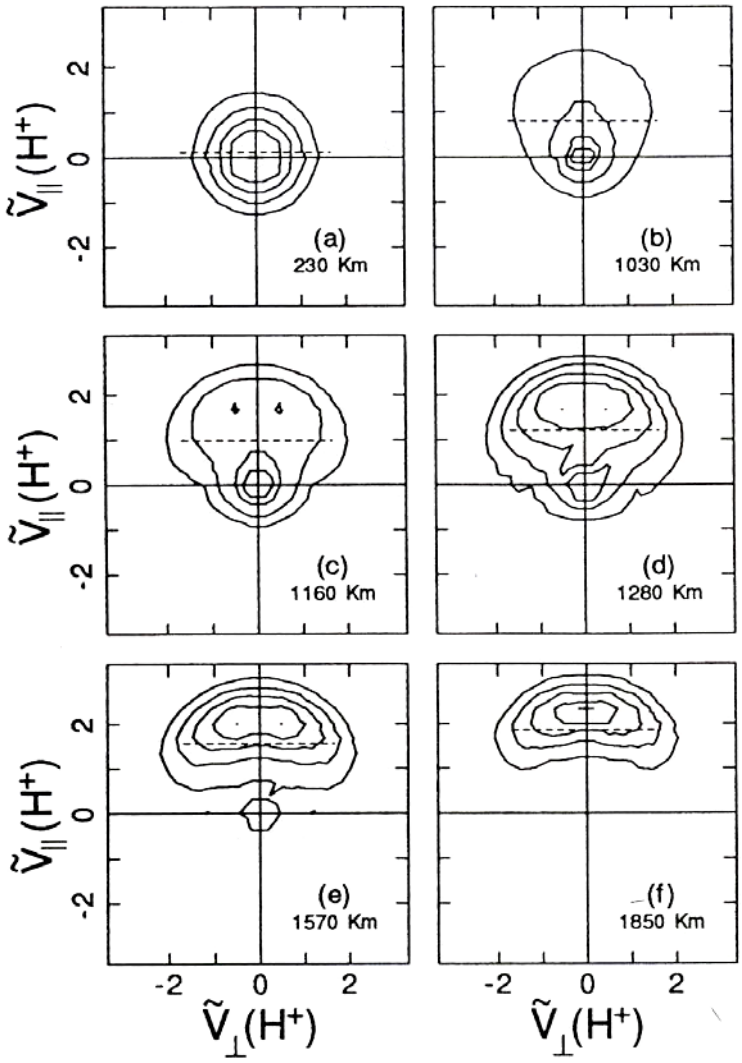

Fig 8. H^+ velocity distributions at six different altitudes, including the lower boundary of the model at 230 km (a), and five altitudes within the transition layer at 1030 km (b), 1160 km (c), 1280 km (d), 1570 km (e), and 1850 km (f). $f(H^+)$is represented by equal-valued contours in the normalized velocity $(\tilde{v}_{\parallel}(H^+),\ \tilde{v}_{\perp}(H^+))$, where $\tilde{v}(H^+) = v(H^+)/[2kT(O^+)/m(O^+)]^{1/2}$. The contour levels are at 0.9 f_{max}, 0.8 f_{max}, 0.7 f_{max}, etc., where f_{max} is the maximum value of $f(H^+)$. The dotted line represents the drift velocity $u(H^+)$. These results have been obtained by a Direct Monte Carlo Simulation (DMCS) by Barakat et al. (1995) for H^+ diffusing through a background O^+ population assumed to be in hydrostatic equilibrium. Note the formation of a secondary peak in the tail of the VDF. The secondary peak is similar to that found in the solutions of the Fokker-Planck equation illustrated in Figures 6 and 7.

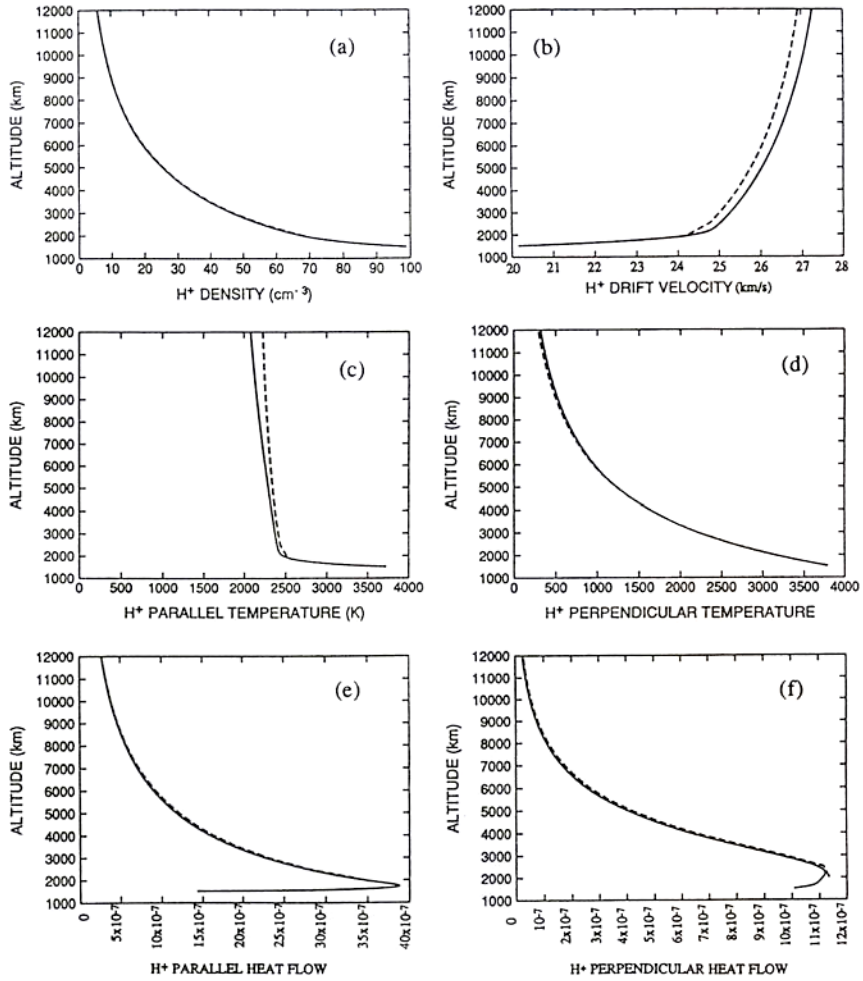

Fig. 9. Comparison of H^+ parameter profiles obtained from semikinetic (dashed curves) and generalized transport (solid curves) models for the supersonic polar wind outflow. Both the semikinetic and generalized transport models were based on a 16-moment bi-Maxwellian based expansion for the H+ velocity distribution function (from Demars and Schunk, 1992).

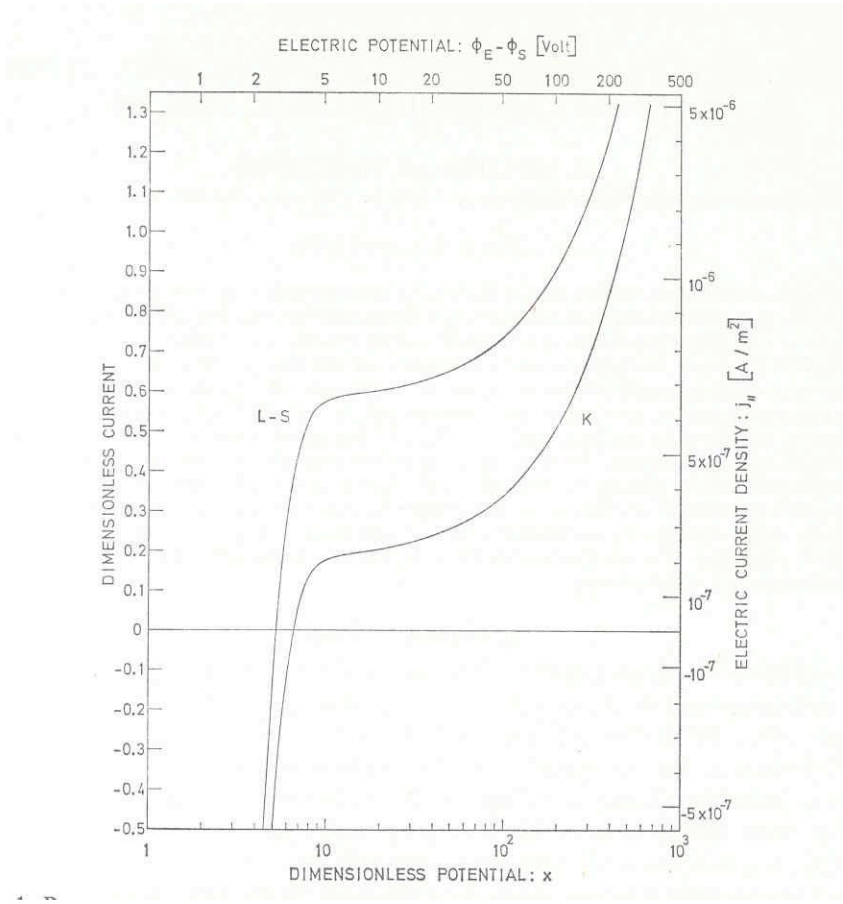

Fig A1. Parallel electric current densities as a function of the electric potential difference between the ionosphere (E) and the plasmasheet (S). In the K-model of Knight (1973) currents of the ions is ignored, and $J_{//} = 0$ for ϕ_E-ϕ_S = 3.4 Volts. In the corresponding more comprehensive L-S model of Lemaire and Scherer (1974 a), the ionic currents are taken into account. Using similar boundary conditions in the ionosphere and plasmasheet the field-aligned current is equal to zero as in the polar wind when ϕ_E-ϕ_S = 2.7 volts (Lemaire and Scherer, 1974b).

the partial